Physics of Fluids

Hole expansion from a bubble at a liquid surface

Cite as: Phys. Fluids **32**, 032108 (2020); https://doi.org/10.1063/1.5139569
Submitted: 21 November 2019 . Accepted: 24 February 2020 . Published Online: 17 March 2020

Sangeeth Krishnan, Baburaj A. Puthenveettil, and E. J. Hopfinger

Physics of Fluids ARTICLE scitation.org/journal/phf

Hole expansion from a bubble at a liquid surface

Cite as: Phys. Fluids 32, 032108 (2020); doi: 10.1063/1.5139569
Submitted: 21 November 2019 • Accepted: 24 February 2020 •
Published Online: 17 March 2020

View Online Export Citation CrossMark

Sangeeth Krishnan,[1,a)] Baburaj A. Puthenveettil,[2,b)] and E. J. Hopfinger[3]

AFFILIATIONS

[1] International Centre for Theoretical Sciences, Tata Institute of Fundamental Research, Bengaluru 560 089, India
[2] Department of Applied Mechanics, Indian Institute of Technology Madras, Chennai 600 036, India
[3] LEGI-CNRS-UGA, BP 53, 38041 Grenoble Cedex 9, France

[a)] Author to whom correspondence should be addressed: sangeeth.soon@gmail.com
[b)] Electronic mail: apbraj@iitm.ac.in

ABSTRACT

For millimetre to micron sized bubbles, floating at the free surface of different low viscosity fluids with different surface tensions, and then collapsing, we study the ensuing expansion of the outer radius of the hole (r_o) at the free surface, as well as its velocity of expansion (u_o). Since the thin film cap of the bubble disintegrates before the hole in it reaches the static rim, the hole expansion at intermediate times occurs as if it initiates at the bubble's static rim of radius R_r; the evolution of r_o then results to be a strong function of gravity, since R_r depends strongly on the bubble radius R. A scaling analysis, which includes the increase in the tip radius due to mass accumulation and the resulting change in the retraction force, along with the gravity effects by considering the hole radius in excess of its initial static radius, $r_e = r_o - R_r$, results in a novel scaling law $r_e/R \sim (t/t_c)^{4/7}$, where $t_c = \sqrt{\rho R^3/\sigma}$ is the capillary time scale; this scaling law is shown to capture the evolution of the hole radii in the present study. The dimensionless velocities of hole expansion, namely, the Weber numbers of hole expansion, $We_o = \rho u_o^2 R/\sigma$, scale as $We_o \sim (t/t_c)^{-6/7}$, independent of gravity effects, matching the observations. We also show that these Weber numbers, which reduce with time, begin with a constant initial Weber number of 64, while the viscous limit of the present phenomena occurs when the bubble Ohnesorge number $Oh = \mu/\sqrt{\sigma\rho R} \simeq 0.24$.

I. INTRODUCTION

Bubbles floating at a liquid surface break after a short time due to hole formation in their upper thin film cap, resulting in an unstable cavity at the surface; the mouth of the cavity expands, creating an expanding hole at the free surface. The phenomenon behind this hole expansion, despite its importance as a unique free surface singularity, remains largely unexplored. Hole formation from free surface bubbles also has practical applications in materials science,[1] cell death in biological reactors,[2] self-assembly of particles,[3] emulsion formation,[4] and many geophysical situations.[5,6] In the present work, we study the expansion of a hole at the surface of different low viscosity fluids with different surface tensions due to the breakup of a bubble of different sizes. Novel scaling laws—different from those observed for the analogous phenomena of neck expansion in drop and bubble coalescence—are observed due to the non-negligible effect of the accumulation of fluid at the retracting tip of the rim, as well as due to the gravitational effect, which occurs through the static shape of the bubble.

Three regions can be identified in the geometry of a bubble at a free surface, namely, the spherical thin film cap, the meniscus projecting above the horizontal liquid surface, and the bubble cavity below the liquid surface; the three surfaces join at a circular ring termed the rim [see Figs. 1(a) and 2(a)]. The thin film cap is of approximately uniform thickness of the order of h = 10 nm–10 μm, while the thickness of the meniscus increases with distance away from the rim.[7] A hole initiates in the thin film cap—with processes similar to those discussed by Vaynblat *et al.*[8] and Thete *et al.*[9]—usually at its base due to gravitational drainage and Marangoni convection,[7] which then expands rapidly over the thin film to reach the rim and then proceeds along the meniscus and then along the horizontal liquid surface [see Figs. 1(b) and 1(e)

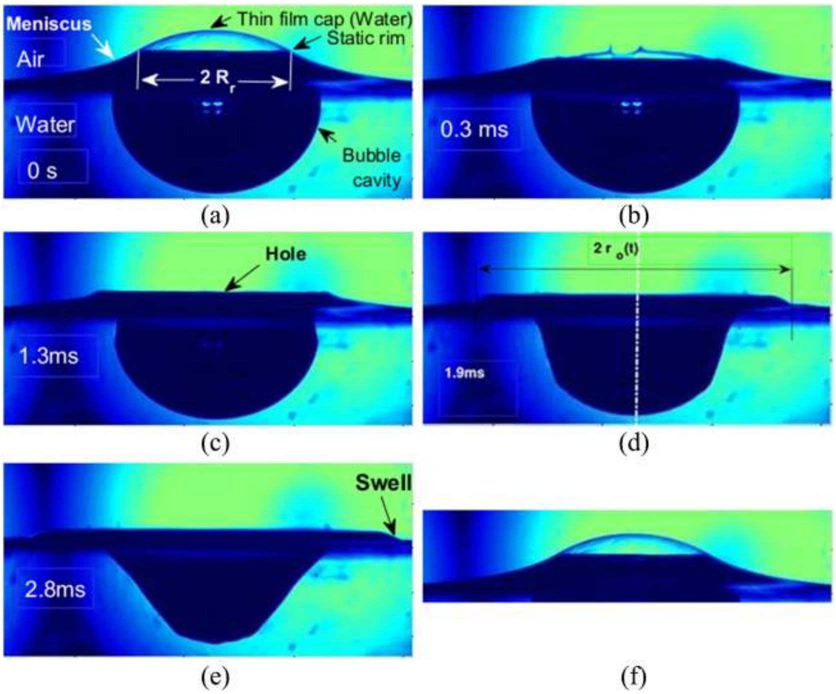

FIG. 1. Hole expansion at the free surface from a bubble of R = 2.32 mm (Bo = 0.73) in water. (a) The static bubble shape, (b) hole expansion in the thin film and its subsequent fragmentation, (c) hole expansion in the meniscus region, and [(d) and (e)] hole expansion along the free surface. Each image width is 9.2 mm. A movie showing a magnified view of hole expansion for the sequence is attached (f). Multimedia view: https://doi.org/10.1063/1.5139569.1

(Multimedia view)]. In up to centimeter sized bubbles, since the variation of h is negligible along the cap, and since the film is of low mass resulting in negligible centrifugal effects, the hole expansion in the spherical thin film cap is known to occur with a constant velocity equal to the well-known Taylor–Culick velocity $U_{TC} = \sqrt{2\sigma/\rho h}$, where σ is the surface tension and ρ is the fluid density.[7,10–13] For a bubble at the surface of a low viscosity fluid like water, U_{TC} in the thin film cap is large, of the order of 50 m/s.[7] When viscous effects become important at the film Ohnesorge number $Oh_f = \mu/\sqrt{\sigma\rho h} \gg 1$, where μ is the dynamic viscosity, the velocity of hole expansion in the film is expected to deviate from U_{TC}.[14] We do not discuss these viscous cases further since our study is for low viscosity fluids; the reader is referred to Refs. 15 and 16 for hole formation in floating bubbles in high viscous fluids.

Once the hole in the thin film encounters the rim, the velocity of its expansion changes from the constant U_{TC}, since unlike the thin film cap, the thickness of the meniscus increases with distance from the rim [see Fig. 2(a)]. These changes have been proposed to be analogous to those occur in the neck expansion in drop or bubble coalescence.[17] In drop coalescence, the neck expansion occurs in an initial viscous regime where the expansion velocity scales as the viscous-capillary velocity $u_{\mu\sigma} = \sigma/\mu$,[18–20] which then later changes to an inertial regime. In bubble coalescence in a viscous outer fluid, a $\sqrt{t}$ scaling of the neck radius has been recently observed during the initial viscous stage as well as during the later inertial stage of neck expansion;[18,21] a similarity solution based explanation for the same has also been provided.[22]

Considering the phenomena similar to the neck expansion in drop coalescence, San Lee *et al.*,[17] in the only available study of long time expansion of the hole at a liquid surface from bubble breakup in low viscosity fluids, observed the dimensionless hole radius $r_h/R \sim (t/t_c)^{1/2}$ at very low bubble sizes (25–49.4 μm), where $t_c = \sqrt{\rho R^3/\sigma}$ is the inertial-capillary time scale, R is the equivalent spherical radius of the bubble, and t is the time. The same scaling is also found for the neck expansion in coalescence of drops at later stages when $r_h > \mu^2/(\rho\sigma)$ so that viscous effects become unimportant.[18,19,23] This scaling occurs when a steady balance of inertial and surface tension forces, $\rho u_h^2 \sim \sigma/(r_h^2/R)$, occurs at the neck during the later stages of neck expansion, assuming that the height of the neck region scales as r_h^2/R, where $u_h = dr_h/dt$ is the velocity of hole expansion.[24] Keller,[25] while extending the Taylor–Culick analysis to a film of varying thickness, specifically for the case of two coalescing bubbles, where the neck height scaled as r_h^2/R, suggested this scaling earlier using a more realistic unsteady momentum balance at the expanding neck. Recently, Soto *et al.*[26] observed a scaling of the neck radius expansion in bubble coalescence with a less than $\sqrt{t}$ dependence on time t. They showed that such a scaling could occur due to the restraining effect of the surface tension force due to the curvature of the expanding neck in the azimuthal direction, as first suggested by Thoroddsen *et al.*[27] for drop coalescence.

However, there are important differences between the hole expansion from a bubble at the free surface and the neck expansion in coalescence of drops or bubbles. The hole expansion in the case of drop or bubble coalescence is essentially a retraction of a bridge of varying thickness from an initial zero radius. In the case of hole expansion in floating bubbles, the expansion proceeds through two regions, initially through the spherical thin film cap of constant thickness and then through the meniscus of varying thickness [see Figs. 1 (Multimedia view) and 2]; the effect of the initial hole expansion in the thin film cap on the retraction of the rim is not

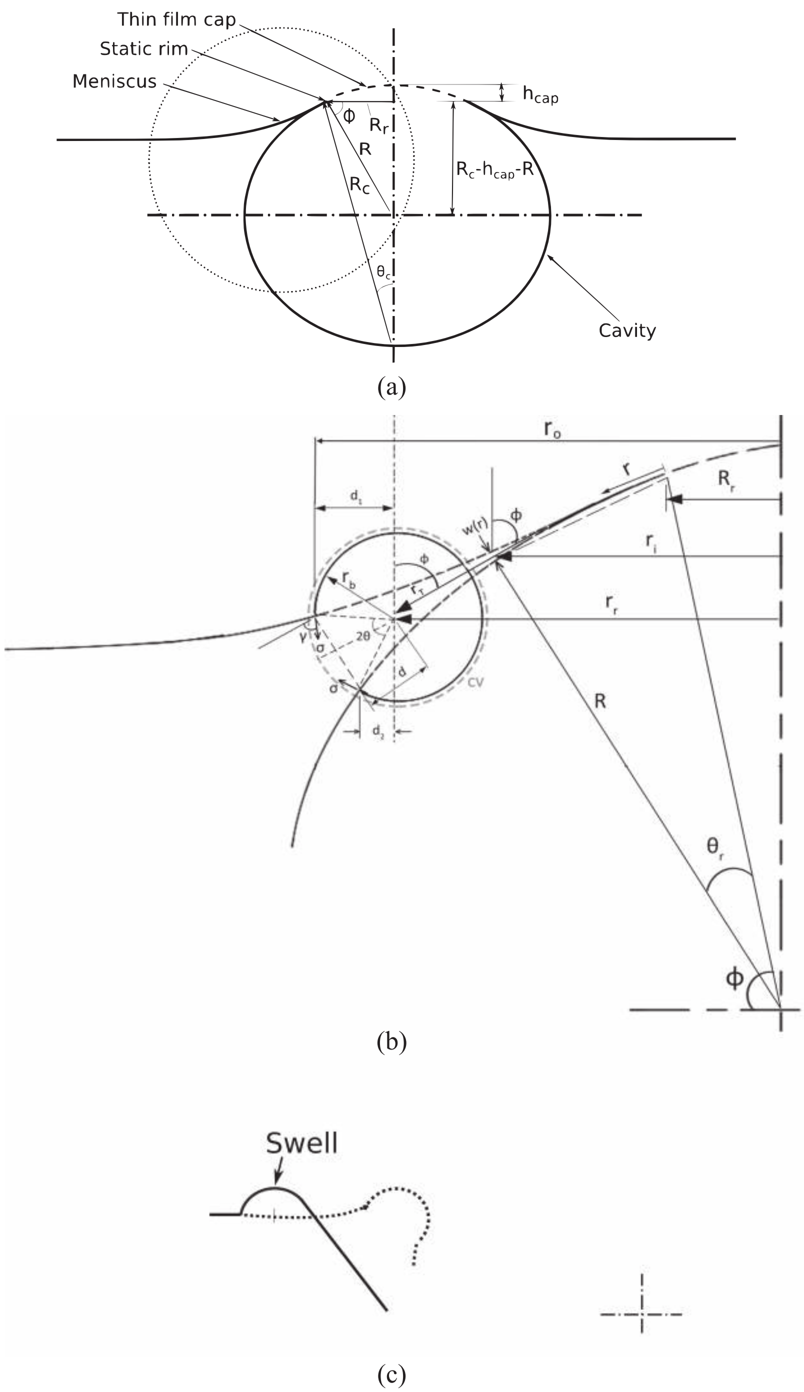

FIG. 2. (a) Schematic of the static bubble at the free surface; (b) zoomed-in view of the region within the dotted circle in (a), showing the retracted rim in the meniscus region with a bulge at its tip, creating an expanding hole at the free surface; and (c) movement of the swell.

clear. Furthermore, the retraction of the rim starts from a finite radius, equal to the static rim radius R_r of the bubble, as shown in Figs. 1(a) (Multimedia view) and 2(a). Such a dependence of the hole expansion on its initial condition R_r, with R_r being a function of the size of the bubble, would mean that the hole expansion in the case of floating bubbles would have additional gravitational effects, not present in drop or bubble coalescence. In addition, for the usual case of bubbles floating in low viscosity fluids, the retraction of the rim would lead to accumulation of fluid at the tip of the rim [see Fig. 2(b)], resulting in the surface curvature at the rim tip to be different from its usually assumed value of R/r_h^2. Even though such an accumulation leading to a toroidal bulge at the rim tip was

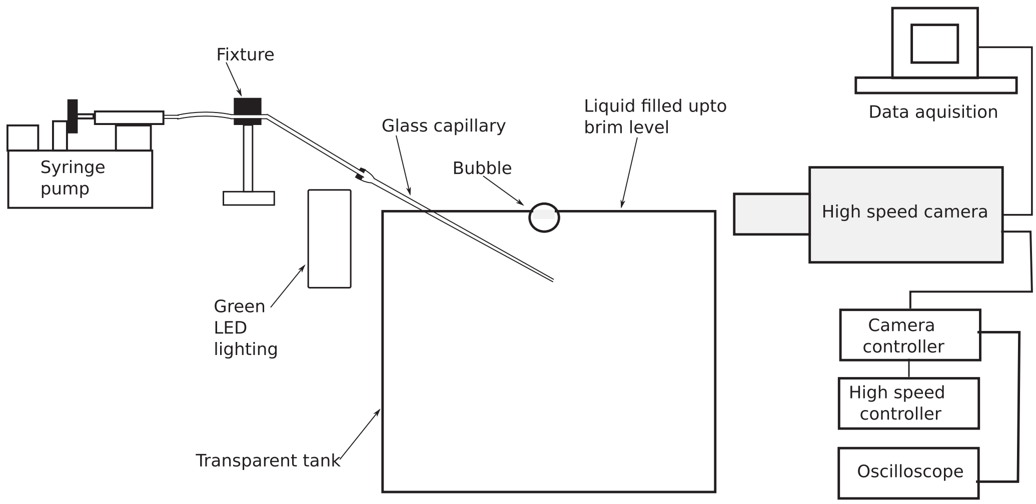

FIG. 3. Schematic of the experimental setup.

proposed earlier[14,24,28] and has been observed in experiments[23] and simulations[16] of drop and bubble coalescence[21] in low viscosity fluids, surprisingly, the effect of this bulge on the scaling of r_h has not been studied extensively.

These differences in the hole expansion from bubbles at a liquid surface from those in the neck expansion of drop or bubble coalescence imply that the proposed $t^{1/2}$ scaling,[17] drawing analogy with drop and bubble coalescence, is likely to be incomplete. The phenomenon has remained largely unexplored, in spite of its importance as a unique free surface singularity in fluid mechanics, along with its numerous applications. The only available study, by San Lee *et al.*,[17] since done over a small range of very small sized bubbles, could not explore the gravitational effects in the hole expansion. In the present study, we study the hole expansion from bubbles of different sizes at the surfaces of different low viscosity fluids having different surface tensions, namely, ethanol, water, and 55% glycerine–water solution, so that the bubble Ohnesorge number $Oh = \mu/\sqrt{\sigma\rho R}$ varies over an order of magnitude $0.003 \le Oh \le 0.05$; $Oh \ll 1$ ensures that viscous effects are negligible in the intermediate times when the hole expands over the horizontal free surface. The equivalent spherical bubble radii of the bubbles are varied over $0.175\ \text{mm} \le R \le 2.32\ \text{mm}$, which along with the surface tension difference in water and ethanol, enable us to investigate the hole expansion over two orders of magnitude range of Bond numbers $0.0042 \le Bo \le 0.74$, where $Bo = \rho g R^2/\sigma$. This range of Bo is further extended by also including the data from San Lee *et al.*[17] at $Bo = 2 \times 10^{-4}$. This large range of Bo helps us to clarify the gravitational effects in hole expansion, which we show to come from the dependence of the initial static rim radius R_r on Bo. Such a conclusion also implies that the initial hole expansion in the spherical film cap, with a velocity U_{TC}, seems to have no influence on the long term evolution of the hole on the horizontal free surface. The hole expansion in the present case occurs over a range of Weber numbers $We_o = \rho u_o^2 R/\sigma$, $1.5 < We_o < 71$, and a range of Reynolds numbers $Re_o = \rho u_o R/\mu$, $22 < Re_o < 2834$, so that the capillary number $Ca_o = We_o/Re_o \ll 1$, where r_o is the outer radius of the hole [see Fig. 2(b)] and $u_o = dr_o/dt$ is the velocity of expansion of r_o; hence, inertia and surface tension dominate the hole expansion process with viscous effects being negligible. In such a situation, in contrast to the proposal of Anthony *et al.*[21] that only the prefactor is affected, we show that the accumulation of the fluid at the tip of the retracting rim changes the scaling of the outer hole radius with time to $r_o \sim t^{4/7}$, different from the usually encountered $t^{1/2}$ scaling.

II. EXPERIMENTAL CONDITIONS

The experiments were conducted on air bubbles of equivalent spherical radii $0.17\ \text{mm} < R < 4.1\ \text{mm}$, produced by pumping air into glass capillaries in a transparent tank, which was filled with the working fluid up to its brim level to avoid meniscus formation. The experimental arrangement is shown in Fig. 3. Two different tanks made of acrylic and glass with cross-sectional areas, $3.5 \times 5\ \text{cm}^2$ and $5 \times 5\ \text{cm}^2$, respectively, were used. Distilled water, ethanol, and glycerol–water mixtures of 48%, 55%, 72%, and 86.8% glycerine concentration (herein after referred to as GW48, GW55, GW72, and GW86.8) were used as the working fluids; the properties of these fluids are given in Table I. Air was pumped into the capillaries by a syringe pump, which was operated at a constant discharge rate within the periodic bubbling regime.[29] Precaution to minimize the

TABLE I. Properties of the working fluids at 20 °C.

	σ kg s^{-2}	ρ kg m^{-3}	μ mPa s
Water	0.072	1000	1.01
Ethanol	0.022	789	1.14
GW48 (30 °C)	0.068	1115	3.9
GW55	0.067	1140	8
GW72 (30 °C)	0.064	1181	16.6
GW86.8	0.062	1226	116.8

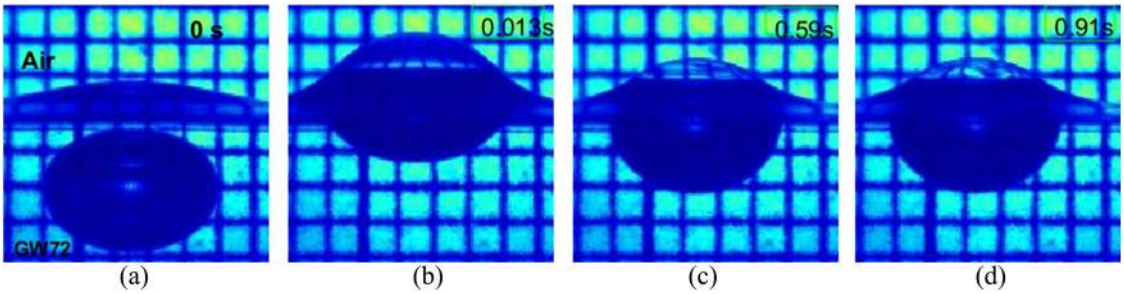

FIG. 4. The interaction of a rising bubble of R = 2.2 mm (Bo = 0.9) with the free surface in GW72. (a) Approach to the free surface, [(b) and (c)] oscillation at the free surface, and (d) the static configuration. For similar Bo, the bubble collapses 4 s after (d). Grid size is 1 mm.

contamination of the interface was taken by changing the liquid after each experimental run. Alignment of the capillary was maintained the same throughout an experiment to avoid variations in bubble size.[30] The experiments were conducted at 20 °C and 30 °C in a temperature controlled laboratory.

The equivalent spherical radius R was calculated from the measured volume of the ellipsoidal bubble, as shown in Fig. 4(a), rising through the fluid after it detaches from the capillary tip. The bubble oscillates for a short time at the free surface [Figs. 4(b) and 4(c)] before becoming stationary [Fig. 4(d)]. Drainage in the thin film cap[31–34] occurs after the bubble becomes stationary to nucleate a hole in the thin film cap. The hole nucleation occurs from stationary conditions since the bubble stays at the free surface for a short time, which varied from 91 ms at $Bo = 4.2 \times 10^{-3}$ to more than 1 s for $Bo > 0.1$, by which time the oscillations are damped out. The hole in the thin film cap leads to its rapid retraction and fragmentation, leaving an open cavity at the free surface [Fig. 1(b) (Multimedia view)]. The mouth of this unstable cavity expands in the radial direction creating an expanding hole at the free surface, bordered by a swell at its periphery [see Figs. 1(c) and 1(e) (Multimedia view)].

The outer radius of this expanding hole at the free surface r_o [see Fig. 1(d) (Multimedia view)] was estimated by measuring the distance between the outer edges of the swells on the left and right sides of the cavity, as shown in Fig. 1 (Multimedia view), and halving this distance. Such measurements of r_o from successive images captured by a high speed camera (La Vision ProHS for ≤19 000 fps and Photron SA4 for ≤100 000 fps) using high intensity LED back lighting gave $r_o(t)$ as a function of time t. The image acquisition rates met the condition that the time between successive frames $t_i = 1/\text{fps} < 1/|du_o/dr|$. The spatial resolution was such that the size of each pixel $p < u_o t_e$, where t_e is the exposure time. The lowest and highest resolutions of the images were 27 μm/pix and 3.4 μm/pix, while the smallest measured r_o was about 100 μm at a resolution of 6 μm/pix. The error in radius measurement was about 2 p.

The velocity of expansion of the hole radius $u_o = dr_o/dt$ was obtained by differentiating curve fits to the r_o vs t data, similar to that shown in Fig. 5. The error in velocity estimation, since a curve fit was used to estimate the gradient of r_o vs t, was $2p/t_f$, where t_f is the time period over which the curve fit was calculated. These estimated errors are shown in the subsequent plots. The origin of time was chosen as the instant when the thin film has disappeared and the static rim is exposed. As shown in Appendix C, the error involved in fixing this origin, due to the finite frame rate of the image acquisition, does not affect the results in any significant way.

III. GRAVITY EFFECTS ON HOLE RADIUS

Figure 5 shows the variation with time t of the expanding outer rim radius $r_o(t)$ for the Bo values investigated in the present experiments ($4.2 \times 10^{-3} \le Bo \le 0.74$), along with the data of San Lee *et al.*[17] at $Bo = 2 \times 10^{-4}$. The increase in outer radii with time follows power laws with exponents varying from 0.56 at the lowest Bo to 0.28 at the highest Bo (see Table II). Figure 6 shows the variation of the radial velocities of expansion of the outer radius $u_o = dr_o/dt$ with time. The hole expansion begins with velocities around 3 m s^{-1}, an order smaller than U_{TC}, and decreases over time. Unlike in the case of Taylor–Culick velocities[10,11] or velocities of cavity mouth opening

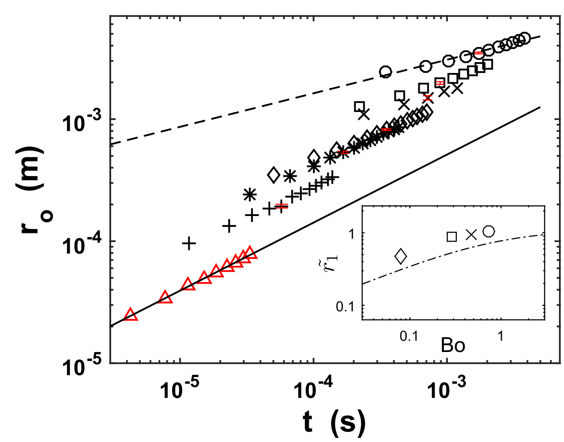

FIG. 5. Variation of the outer hole radius $r_o(t)$ with time t. For water: +, R = 0.175 mm, $Bo = 4.2 \times 10^{-3}$; $\ast$, R = 0.47 mm, $Bo = 3 \times 10^{-2}$; □, R = 1.47 mm, $Bo = 2.9 \times 10^{-1}$; and ◯, R = 2.32 mm, $Bo = 7.4 \times 10^{-1}$. For other fluids: ◊, R = 0.7 mm, $Bo = 8.3 \times 10^{-2}$, GW55; ×, R = 1.16 mm, $Bo = 4.7 \times 10^{-1}$, ethanol; △, R = 25 μm, $Bo = 2 \times 10^{-4}$, ethanol from San Lee *et al.*;[17] - -, $0.026\, t^{0.565}$; and –, $0.021 t^{0.275}$. The inset shows the variation of $\tilde{r}_1 = r_1/R$ with Bo, where r_1 is the first data point at each Bo in the main figure; -.-, (1).

TABLE II. Bubble sizes, the range of dimensionless numbers, and the variation of the outer hole radius with time in the present experiments. $Bo = \rho g R^2/\sigma$, $Oh = \mu/\sqrt{\sigma\rho R}$, $We_o = \rho u_o^2 R/\sigma$, and $Re_o = \rho u_o R/\mu$.

	R (m)	Bo	Oh	We_o	Re_o	Best fit r_o (m)
Ethanol △	25×10^{-6}	2×10^{-4}	0.055	1.5–9	22–55	$0.024t^{0.558}$
Water +	0.175×10^{-3}	4.2×10^{-3}	0.009	4–36.8	224–677	$0.029t^{0.506}$
Water ∗	0.47×10^{-3}	3×10^{-2}	0.006	7.3–65.3	496–1480	$0.04t^{0.495}$
GW55 ◊	0.71×10^{-3}	8.3×10^{-2}	0.034	8–71	83–247	$0.028t^{0.445}$
Water □	1.47×10^{-3}	2.9×10^{-1}	0.003	7.6–49.4	892–2275	$0.026t^{0.361}$
Ethanol ×	1.16×10^{-3}	4.7×10^{-1}	0.008	13.8–51.5	465–898	$0.015t^{0.313}$
Water ○	2.32×10^{-3}	7.4×10^{-1}	0.003	6.6–48.5	1045–2834	$0.021t^{0.275}$

due to drop impact,[35] both of which occur at constant velocities with time, the present velocities at different Bo decrease with a common power law exponent of $-3/7$. This common slope in Fig. 6 is in contrast to the varying slopes with Bo that we observe for the variation of r_o with t in Fig. 5. The lower the bubble size, the larger the velocity of hole expansion.

The most prominent feature in Fig. 5 is the vertical shift of r_o vs t with Bo, implying that the hole expansion for each Bo starts from different outer radii r_1, where r_1 is the first data point at each Bo in Fig. 5. This behavior is unlike that in the case of drop coalescence,[24] film retraction,[10] or drop impact,[35] where the initial radius of the bridge is always zero at all Bo. In contrast, in free surface bubbles, the radii of the hole r_1, from which the hole expansion proceeds with power laws in Fig. 5, increase with Bo; r_1 is, hence, a strong increasing function of Bo. This dependence of r_1 on Bo has to be first quantified before we obtain a scaling for $r_o(t)$; we now proceed to do so.

The inset in Fig. 5 shows the variation of $\tilde{r}_1 = r_1/R$ with Bo. This figure also shows the theoretical variation of the dimensionless static

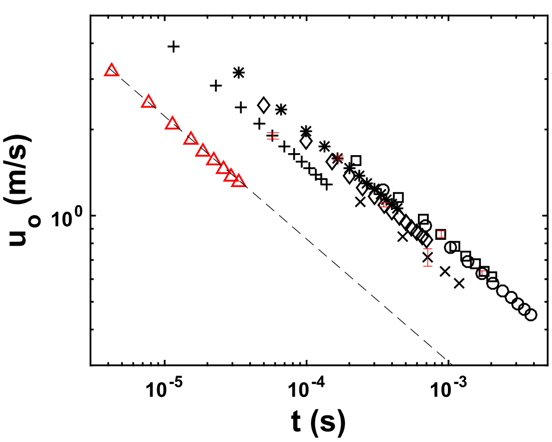

FIG. 6. Variation of the radial velocity of the outer hole $u_o(t)$ with time t. For water: +, R = 0.175 mm, $Bo = 4.2\times10^{-3}$; ∗, R = 0.47 mm, $Bo = 3\times10^{-2}$; □, R = 1.47 mm, $Bo = 2.9\times10^{-1}$; and ◯, R = 2.32 mm, $Bo = 7.4\times10^{-1}$. For other fluids: ◊, R = 0.7 mm, $Bo = 8.3\times10^{-2}$, GW55; ×, R = 1.16 mm, $Bo = 4.7\times10^{-1}$, ethanol; △, R = 25 μm, $Bo = 2\times10^{-4}$, ethanol from San Lee *et al.*;[17] and - -, $0.016t^{-3/7}$.

rim radius $\tilde{R}_r = R_r/R$,

$$\tilde{R}_r = \sqrt{\frac{4}{3} - 2\left(\frac{1}{Bo} + \frac{1}{Bo^2}\right) + \sqrt{\frac{-4}{3Bo^2} + \frac{8}{Bo^3} + \frac{4}{Bo^4}}}, \tag{1}$$

given by Puthenveettil *et al.*[36] The variation of $\tilde{r}_1$ with Bo is the same as that of $\tilde{R}_r$ with Bo, given by (1), the reasons for which are given in Appendix A. Hence, even though the hole formation initiates in the thin film cap above the bubble cavity, the long term expansion of the hole on the free surface behaves as if it initiates at the static rim. The film cap seems to have no effect on the subsequent hole expansion process since the film cap, which has a very low mass, disintegrates before the hole in the film cap reaches the rim (see Appendix B). Since the initial radius of the hole r_1 is a function of Bo, with the same functionality as R_r given by (1), the evolution of the outer radius $r_o(t)$ now becomes a function of Bo.

To account for such Bo effects on r_o through its dependency on R_r, we now define the hole radius in excess of the static rim radius as

$$r_e = r_o - R_r. \tag{2}$$

Figure 7 shows the variation of r_e with time for all Bo. The data at different Bo now have the same power law exponent, which is approximately equal to 4/7, as shown by the dashed line in this figure. Even though the power law exponent of 4/7 is close to the exponent of 1/2 seen in bridge expansion during drop coalescence,[24] the plot of $r_e/t^{1/2}$ vs t in the inset of Fig. 7 shows that the excess hole radius r_e in bubble collapse at the free surface clearly does not scale as $t^{1/2}$. As shown in Appendix C, this 4/7 scaling is also not an artifact of the uncertainty in the origin of time due to the finite frame rate of imaging and, hence, the 4/7 scaling appears to originate due to real physical reasons which we discuss below. The monotonic increase in r_o with an increase in Bo (shown in Fig. 5) is not shown in Fig. 7. The curves in Fig. 7 are, however, still offset by different prefactors, since the varying capillary effects during the course of hole expansion are yet to be accounted for in Fig. 7. We now present a scaling analysis to account for such varying capillary effects with time in the hole expansion process, which then explains the 4/7 scaling of r_e and collapses all the data on to a single dimensionless power law.

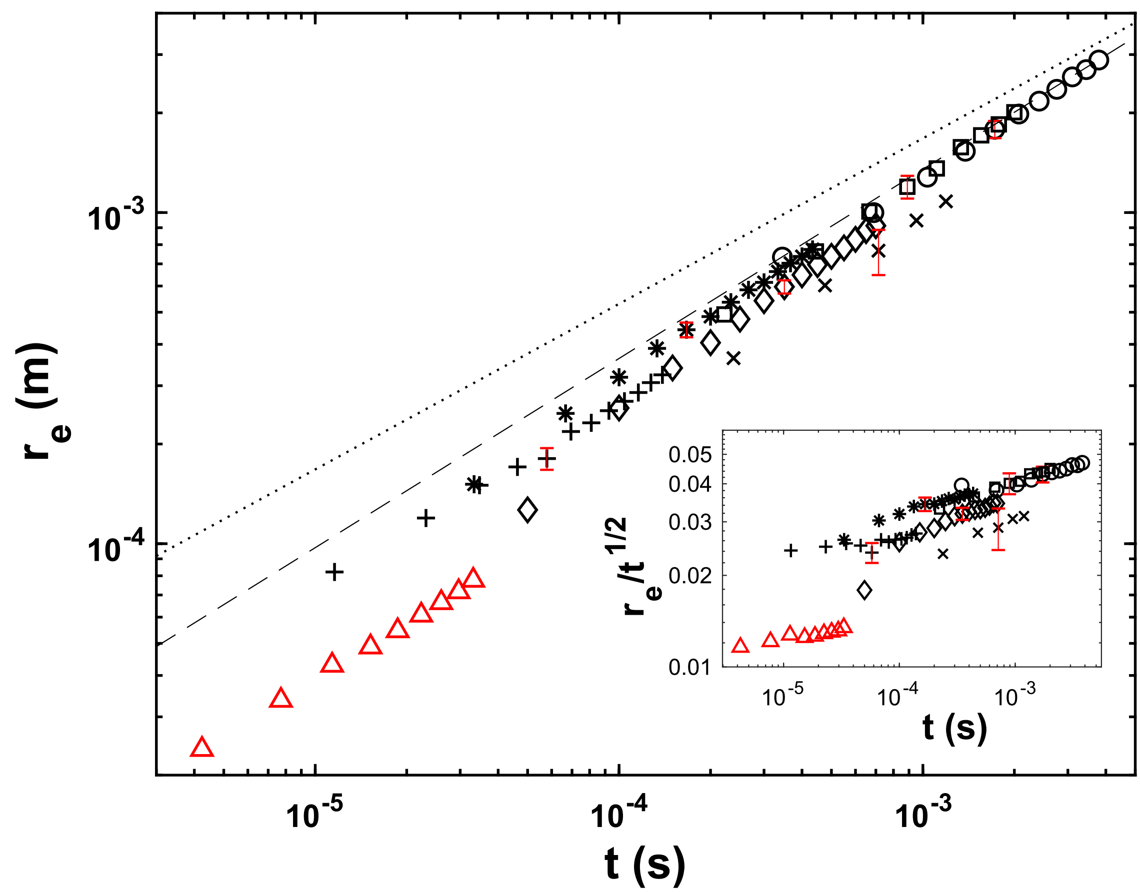

FIG. 7. Variation of the excess outer radius $r_e(t)$ (2) with time t. The inset shows the variation of r_e normalized with $\sqrt{t}$, the inertial-capillary coalescence scaling.[24] For water: +, R = 0.175 mm, Bo = 4.2 × 10^{-3}; ∗, R = 0.47 mm, Bo = 3 × 10^{-2}; □, R = 1.47 mm, Bo = 2.9 × 10^{-1}; and ◯, R = 2.32 mm, Bo = 7.4 × 10^{-1}. For other fluids: ◊, R = 0.7 mm, Bo = 8.3 × 10^{-2}, GW55; ×, R = 1.16 mm, Bo = 4.7 × 10^{-1}, ethanol; △, R = 25 μm, Bo = 2 × 10^{-4}, ethanol from San Lee *et al.*;[17] - -, $r_e = 0.07\, t^{4/7}$; and . . ., $r_e = 0.053 t^{1/2}$.

IV. SCALING ANALYSIS

Consider a static bubble at the free surface of a liquid whose schematic is shown in Fig. 2(a), where the rim has an initial static radius R_r. The static bubble undergoes thin film cap breakup and then hole expansion so that the rim expands to have a radius $r_r(t)$ at an intermediate stage of hole expansion, the schematic of which is shown in Fig. 2(b). Accumulation of mass at the tip of the rim results in an expanding radius of the bulge $r_b(t)$ at the tip of the rim, which will be at a distance r_T from the initial static location of the rim tip [see Fig. 2(b)]; the corresponding no-bulge case is discussed in Appendix D. The measured outer radius is $r_o = r_r + r_b$. Some part of the bulged tip travels along the horizontal free surface as a swell [see Fig. 2(c)], whose radius we assume to evolve in the same way as r_b. We now consider an integral analysis of the retracting and growing bulge to obtain the experimentally observed scaling law; the same scaling law is also obtained by a modified Euler equation approach, as shown in Appendix E.

We consider a control volume (CV) coinciding with the retracting and expanding bulge of radius $r_b(t)$, as shown in Fig. 2(b). The resulting CV is, hence, of the form of a torus having a radius r_r and a radius of cross section r_b. Mass balance of the CV results in

$$\int_0^{r_T} 2\pi r_i w(r) dr = \pi r_b^2 2\pi r_r, \tag{3}$$

implying that the fluid in the film that retracted from $r = 0$ to r_T gets accumulated in a torus of radius r_r, whose radius of the cross section is r_b. The momentum balance in the r direction of the expanding and decelerating CV results in

$$\rho \frac{d}{dt}\int_V \bar{v}_r dV = \Sigma \bar{F}_r - m\bar{a}_r - \int_S \bar{v}_r \rho \bar{v}_r \cdot d\bar{S}, \tag{4}$$

where $\bar{v}_r$ is the relative velocity in the r direction of the fluid inside the CV with respect to the decelerating CV, V is the volume of the CV, $\bar{F}_r$ is the force in the r direction, m is the mass of the fluid in the CV, $\bar{a}_r$ is the acceleration of the CV in the r direction, and $\bar{S}$ is the surface area of the CV.

Assuming that the fluid in the bulge moves with the same velocity as the bulge

$$\int_V \overline{v}_r dV = 0. \tag{5}$$

This assumption is justified at low Oh since velocity gradients inside the bulge are negligible in such a case, as the simulations of Savva and Bush[16] show; the present case of $Oh \sim 10^{-3}$ (see Table II) satisfies this condition.

The component of the surface tension force at the bulge along r is $F_\sigma = \sigma\cos\gamma(2\pi r_r + d_1) + \sigma\cos\gamma(2\pi r_r + d_2)$. This force balances the force due to the pressure inside the bulge $F_p = s\sigma/r_b$, where

$$s = 4\pi r_r r_b \theta \tag{6}$$

is the surface area of the torus over the angle 2θ, as shown in Fig. 2(b). Hence,

$$F_p = 4\pi r_r \sigma\theta = F_\sigma. \tag{7}$$

The component of the weight of the bulge in the r direction, $F_g = 4\pi r_b^3 \rho g\cos\phi/3$, can be neglected since $F_\sigma/F_g = R^2 r_r 3\theta/(r_b^3\cos\phi Bo) \gg 1$ because $Bo < 1$, $R^2 r_r/r_b^3 \gg 1$, and ϕ is close to $\pi/2$. The viscous resistance at the surface of the CV is negligible due to the stress free condition at the bulge–air interface, and the viscous resistance in the neck region of the bulge is negligible since the gradients of velocity at the neck are negligible at low Oh. Then, the net force in the r direction is $\Sigma\overline{F}_r \simeq F_\sigma$, and the surface tension force in the r-direction is given by (7).

Using (3), the fictitious force due to the deceleration of the CV,

$$m\overline{a}_r = \rho\pi r_b^2 2\pi r_r \frac{d\overline{u}_T}{dt}, \tag{8}$$

where

$$u_T = \frac{dr_T}{dt} \tag{9}$$

is the retraction velocity along r_T, with r_T being the distance from the initial static rim position to the center of the swell at the tip of the retracting rim, as shown in Fig. 2(b). From the geometry shown in Fig. 2(b),

$$\sin\phi = \frac{r_r - R_r}{r_T}. \tag{10}$$

Since $\sin\phi \simeq 1$, for the case of retraction that we consider

$$r_r \simeq r_T + R_r. \tag{11}$$

The bulge radius r_b in (8) scales similar to that in the case of bridge expansion in drop coalescence,

$$r_b = c_1 \frac{r_T^{3/2}}{\sqrt{R}}, \tag{12}$$

as obtained by Eggers, Lister, and Stone,[24] where c_1 is a constant. As shown in Appendix F, Eq. (12) can also be obtained by a mass balance of the retracting rim to give $c_1 = 1/2\sqrt{\pi}$ from (F11). Replacing r_r and r_b in (8) with (11) and (12), respectively, we obtain

$$m\overline{a}_r = 2(\pi c_1)^2 \frac{\rho r_T^4}{R}\left(1 + \frac{R_r}{r_T}\right)\frac{d\overline{u}_T}{dt}. \tag{13}$$

Here, $R_r/r_T \ll 1$ in (13) for the intermediate regime of hole expansion that we consider for $Bo < 1$. Hence, by dropping R_r/r_T, rewriting $d\overline{u}_T/dt$ as $u_T d\overline{u}_T/dr_T$ and using the value of c_1 from (F11), (13) simplifies to

$$m\overline{a}_r \simeq \frac{\pi}{2}\frac{\rho r_T^4}{R} u_T \frac{du_T}{dr_T}. \tag{14}$$

Assuming that the fluid in the film outside the bulge to be stationary, which results in $v_r = -u_T$ over the surface s, whose expression is given by (6), the net efflux of momentum in (4) becomes

$$\int_S \overline{v}_r \rho \overline{v}_r \cdot d\overline{S} = \rho u_T^2 4\pi r_r r_b \theta. \tag{15}$$

Using (5), (7), (14), and (15) in (4) and simplifying, we obtain a Bernoulli differential equation,

$$\frac{du_T}{dr_T} + P_1 u_T - \frac{Q_1}{u_T} = 0, \tag{16}$$

where

$$P_1 = \frac{8 r_b r_r R\theta}{r_T^4} \quad\text{and}\quad Q_1 = \frac{8\sigma r_r R\theta}{\rho r_T^4}. \tag{17}$$

Using (11) in (17), we obtain

$$P_1 \simeq \frac{8 r_b R\theta}{r_T^3}\left(1 + \frac{R_r}{r_T}\right) \quad\text{and}\quad Q_1 \simeq \frac{8\sigma R\theta}{\rho r_T^3}\left(1 + \frac{R_r}{r_T}\right). \tag{18}$$

Since $R_r/r_T \ll 1$, (18) reduces to

$$P_1 \simeq \frac{8 r_b R\theta}{r_T^3} \quad\text{and}\quad Q_1 \simeq \frac{8\sigma R\theta}{\rho r_T^3}. \tag{19}$$

In (19), for small θ,

$$\theta \simeq \sin\theta = \frac{(w/2)|_{r_T+d}}{r_b} \simeq \frac{(w/2)|_{r_T+r_b}}{r_b}, \tag{20}$$

when $(w/2)|_{r_T+d}/r_b \ll 1$. Using (F6) in (20), we obtain

$$\theta \simeq \frac{1}{2}\frac{(r_T + r_b)^2}{R r_b}. \tag{21}$$

Substituting (21) in (19), we obtain

$$P_1 \simeq \frac{4}{r_T}\left(1 + \frac{r_b}{r_T}\right)^2 \quad\text{and}\quad Q_1 \simeq \frac{4\sigma}{\rho r_T r_b}\left(1 + \frac{r_b}{r_T}\right)^2. \tag{22}$$

Since $r_b/r_T \ll 1$ in our case, (22) reduces to

$$P_1 \simeq \frac{4}{r_T} \quad\text{and}\quad Q_1 \simeq \frac{4\sigma}{\rho r_T r_b}. \tag{23}$$

Since r_b in the expression for Q_1 in (23) is given by (F10), Q_1 can be expressed as

$$Q_1 = \frac{4}{c_1}\frac{\sigma}{\rho}\sqrt{\frac{R}{r_T^5}}. \tag{24}$$

Using the standard method of solving the Bernoulli differential equation by transforming the equation into a linear ordinary differential equation (see Boas[37]), the solution for (16), with P_1 and Q_1 given by (23) and (24), is

$$\frac{u_T}{u_c} = c_2\left(\frac{R}{r_T}\right)^{3/4}, \tag{25}$$

after assuming the integration constant to be zero, where $u_c = \sqrt{\sigma/\rho R}$ is the capillary velocity and $c_2 = 4/\sqrt{13c_1} = 2.1$. Substituting (9) in (25), rearranging, and integrating, along with using $r_T \to 0$ as $t \to 0$, we obtain the dimensionless distance of rim tip retraction, $\tilde{r}_T = r_T/R$, as

$$\tilde{r}_T = c_3 t^{*4/7}, \tag{26}$$

where $t^* = t/t_c$ with $c_3 = (7/\sqrt{13c_1})^{4/7} = 2.1$.

A. Expansion of the hole radius

Equation (26) is strictly valid in the initial stages of hole opening where the rim moves in the direction of r_T. In the later stages, the swell moves horizontally; our measurements of the outer rim radius r_o are mostly in this regime. However, as shown in Fig. 2(b),

$$r_T + r_b \simeq \frac{r_o - R_r}{\sin\phi}. \tag{27}$$

Since the increase in r_b during our measurement time of r_o is small because $dr_b/dt \ll dr_o/dt$, as shown in Appendix G, $r_T + r_b \sim r_T$. Furthermore, for the case when the ridge moves horizontally along the free surface $\phi \simeq 90^\circ$ so that $\sin\phi \simeq 1$. Using these scales in (27) implies that

$$r_T \simeq r_o - R_r = r_e, \tag{28}$$

and the path traveled by the swell when it is moving horizontally scales approximately as the excess rim radius r_e. Hence, we expect (26) to be valid as a scaling law for r_e when the swell moves horizontally along the free surface. In other words, from (26) and (28), the dimensionless excess hole radius scales as

$$\tilde{r}_e \simeq c_3\, t^{*4/7}, \tag{29}$$

where $\tilde{r}_e = r_e/R$, with the excess hole radius r_e given by (2). Dimensionally, this new scaling could be expressed as

$$r_e = c_3\left((u_c t)^4 R^3\right)^{1/7}, \tag{30}$$

a function of two length scales $u_c\, t = \sqrt{\sigma t^2/\rho R}$ and R.

Figure 8 shows the variation of the dimensionless excess hole radius $\tilde{r}_e$ with the dimensionless time t^*. The datasets for different Bo collapse well on to the line

$$\tilde{r}_e = 2.7\, t^{*4/7} \tag{31}$$

for the range of Bond numbers $1 \times 10^{-4} < Bo < 1$, in agreement with (29); note that the experimental value of the prefactor c_3 in (31) also matches well with the theoretical value of 2.1 in (29). The collapse is not perfect possibly because the difference between the actual curved path of travel of the swell and the distance $\acute{r}_T$, which is a function of Bo, is neglected in the present analysis. Furthermore, there could be a small contribution to the measured r_o due to the expansion of the swell (see Appendix G), which is neglected in the present analysis. Despite these approximations, (29) captures the scaling of the expansion of the hole from bubble collapse at a free surface remarkably well.

It needs to be noted that the present scaling (31) is different from the conventional $t^{1/2}$ inertial scaling proposed first by Keller[25] for the case of neck expansion for coalescing bubbles. As shown in Appendix H, the analysis by Keller,[25] as well as that by Culick[11] for films of constant thickness, implicitly assumes that there is no bulge formation at the retracting rim tip. We show in Appendix D that the present analysis retrieves the $t^{1/2}$ scaling in the limiting case of hole expansion without bulge formation at the retracting rim tip. Although fundamentally different from the present problem, the same 4/7 scaling exponent of the horizontal length scale with time has been found in film rupture over solid substrates for power law fluids when inertia dominates,[38] for the length scale in the neighborhood of an inertia driven microjet due to a collapsing cavity,[39] and in the inertial collapse of holes.[40]

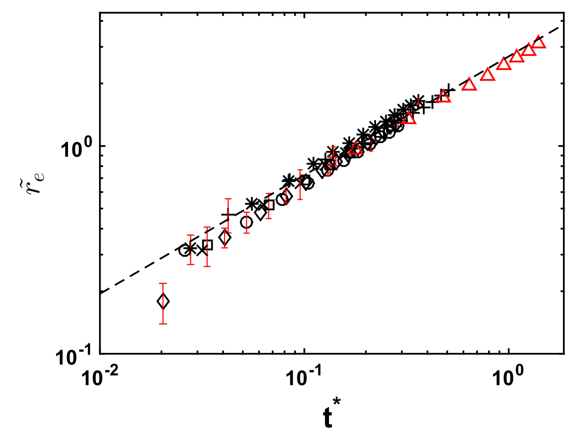

FIG. 8. Variation of the dimensionless excess outer radius of the rim $\tilde{r}_e = r_e(t)/R$ with the dimensionless time $t^* = t/t_c$. For water: +, R = 0.175 mm; $\ast$, R = 0.47 mm; ◯, R = 2.32 mm; and □, R = 1.47 mm. For other fluids: ◊, R = 0.7 mm, GW55; ×, R = 1.16 mm, ethanol; △, R = 25 μm, ethanol from San Lee *et al.*;[17] and - -, $\tilde{r}_e = 2.7t^{*4/7}$ (31).

B. Velocity of hole expansion

The scaling (29) implies that the dimensionless outer radius

$$\tilde{r}_o \simeq c_3\,(t/t_c)^{4/7} + \tilde{R}_r. \tag{32}$$

On the RHS of (32), the only term that has gravitational dependence, through its dependence on Bo shown by (1), is the dimensionless static rim radius $\tilde{R}_r$. The gravitational dependence of $\tilde{r}_o$ is, hence, due to the dependence of its initial condition, namely, $\tilde{R}_r$ on gravity. $\tilde{R}_r$, which is independent of time, also occurs as an addition to the first, time dependent, capillary term in (32). Such a gravitational dependence of $\tilde{r}_o$, since it is of the form of an addition of an initial condition that is constant with respect to time, will vanish when we calculate the velocity of hole expansion $u_o = dr_o/dt$, making u_o independent of gravity effects. This is also the reason why the same slopes are observed for the variation of u_o with t in Fig. 6.

Differentiating (29) with respect to time yields the Weber number of hole expansion $We_o = \rho u_o^2 R/\sigma$ as

$$We_o \simeq c_4\, t^{*-6/7}, \tag{33}$$

where $c_4 = (4c_3/7)^2 = 1.4$. Figure 9 shows the variation of We_o with t^*; the data collapse fairly well to

$$We_o = 2.5\, t^{*-6/7}, \tag{34}$$

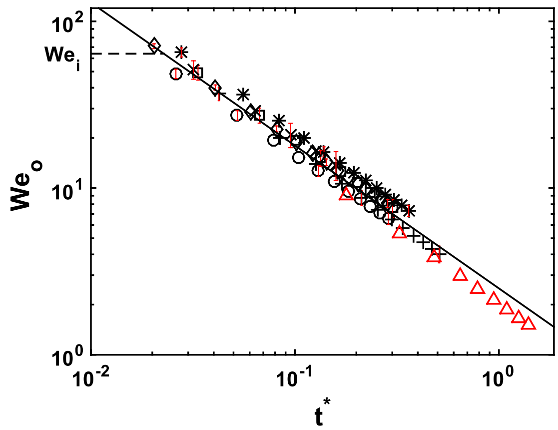

FIG. 9. Variation of the Weber number of expansion of the outer radius of the hole We_o with the dimensionless time $t^* = t/t_c$. For water: +, R = 0.175 mm; $\ast$, R = 0.47 mm; ◯, R = 2.32 mm; and □, R = 1.47 mm. For other fluids: ◊, R = 0.7 mm, GW55; ×, R = 1.16 mm, ethanol; △, R = 25 μm, ethanol from San Lee *et al.*;[17] —, $We_o = 2.5t^{*-6/7}$ (34); and - -, We_i = 64 (38).

in agreement with (33). The theoretical value of c_4 in (33) is in agreement with the value obtained from experiments in (34). The dimensionless scaling (33) implies that

$$u_o = c_5\,(u_c{}^4(R/t)^3)^{1/7}, \tag{35}$$

a function of two velocity scales u_c and R/t, where $c_5 = \sqrt{c_4} = 1.2$. The dependence of We_o on the excess hole radius can be obtained from (29) and (33) as

$$We_o = c_6\,\tilde{r}_e{}^{-3/2}, \tag{36}$$

where $c_6 = (4/7)^2 c_3^{7/2} = 4.4$.

C. Initial velocity of hole expansion

The velocity scaling (35) implies that $u_o \to \infty$ when the initiation of hole expansion occurs at $t \to 0$. However, the present scaling is only valid from the time when a bulge of fluid has formed at the tip of the retracting rim, which occurs after a small time from the initiation of hole expansion. At the very beginning of hole expansion, after the thin film cap has fragmented, when $r_T < R_{\mu\sigma} = \mu^2/\sigma\rho$, viscous effects will be prevalent and no bulge is expected to form at the rim tip.[14,16] In this viscous region, the hole expansion velocity is expected to follow either $u_o \sim u_{\mu\sigma} = \sigma/\mu$, as in the case of drop coalescence,[19] or $u_o \sim \sqrt{u_{\mu\sigma}R/t}$, as in the case of bubble coalescence.[18,21,22] It is also possible that there is no direct transition between an initial viscous and a later inertial regime, as shown by Castrejón-Pita *et al.*[41] for the case of breakup of filaments. In any case, the length scale $R_{\mu\sigma}$ is of the order of nanometers in usual fluids, and this regime is, hence, not observed in our measurements that have a maximum resolution of 3.4 μm/pix.

Beyond this initial viscous region, before the temporal decay of velocity predicted by (35) sets in with accumulation of fluid at the rim tip, in a short region for $r_T > R_{\mu\sigma}$, we expect the spatial acceleration to be much larger than the temporal acceleration. This region, being the first observable region, we denote as the initial region with a subscript i. In this region, we measure u_{T_i}, the initial rim tip retraction velocity in the direction of r_T, as described in Appendix I. Figure 10 shows the variation of the Capillary number based on u_{T_i}, $Ca_i = \mu u_{T_i}/\sigma$, with Oh, where the error bars show the error in Ca_i due to the error in velocity measurement $\delta u_{T_i} \simeq 2p/t_i$. This figure shows that

$$Ca_i \simeq 8\,Oh, \tag{37}$$

implying that $u_{T_i} \simeq 8\,u_c$. In other words,

$$We_i \simeq 64, \tag{38}$$

where $We_i = \rho u_{T_i}{}^2 R/\sigma$ is the initial Weber number of rim tip retraction, showing the inertial dominance in the initial hole expansion. This initial Weber number We_i is shown in Fig. 9; the Weber numbers of hole expansion decrease with time as per (33) starting from We_i. These initial velocities, and the corresponding Weber numbers We_i, seem to be independent of U_{TC} since, as shown in Appendix B, the thin film cap disintegrates before the hole in the thin film cap reaches the static rim.

Figure 10 shows the variation with Oh of the estimated values of the Capillary numbers of film retraction in the spherical thin film cap, $Ca_{TC} = \mu U_{TC}/\sigma$, for bubbles in water, calculated for the same radii as our bubbles in experiments with water. Ca_{TC} are an order of magnitude larger than Ca_i and have a different dependence on Oh compared to (37). The velocities of hole expansion decrease from U_{TC} in the thin film cap to u_{T_i} at the beginning of hole expansion from which point onward the hole expansion obeys (35). The variation of Ca_{TC} with Oh, shown in Fig. 10, could be obtained by using $U_{TC} = \sqrt{2\sigma/\rho h}$ and $h = R^2/20$ m for water[7] in the expression for Ca_{TC} to obtain

$$Ca_{TC} = \sqrt{\frac{40}{R_{\mu\sigma}}}\,Oh^2, \tag{39}$$

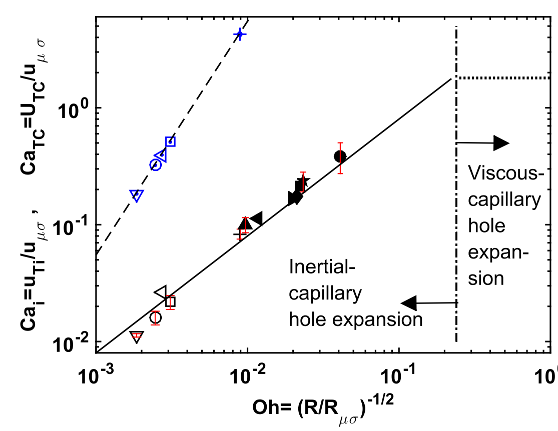

FIG. 10. Variation of the dimensionless initial hole expansion velocity (41) with Ohnesorge number. ◁, R = 1.9 mm, water; ▽, R = 4.08 mm, water; ◀, R = 1.45 mm, GW48 (30 °C); ▲, R = 2.1 mm, GW48 (30 °C); ■, R = 1.66 mm, GW55; ⧫, R = 1.85 mm, GW55; ▶, R = 2.11 mm, GW55; ⋆, R = 1.52 mm, GW55; and •, R = 2.17 mm, GW72. The symbols ◯, □, and + denote the same bubbles as in Fig. 5. —, Ca_i = 8 Oh (37); –.–, the vertical line denoting $Re_i \simeq 1$; and . . ., Ca_i = 1.8. The blue colored symbols with inside dots represent the Capillary number based on U_{TC} and Ca_{TC}, calculated for the cases shown by the corresponding hollow or solid symbols. – –, $Ca_{TC} = \mu U_{TC}/\sigma = \sqrt{40/R_{\mu\sigma}}\,Oh^2$ (39).

where 40 is in meters; (39) is shown by the dashed line in Fig. 10. Since (39) also implies that $U_{TC} = \sqrt{40/R}\, u_c$, similar to the case of initial velocity given by (38), the Weber numbers based on U_{TC} will be $\sqrt{40/R}$, independent of viscosity.

D. Viscous effects in hole expansion

The condition for viscous effects in hole expansion can now be obtained as follows. Neglecting temporal acceleration in the initial region discussed in Sec. IV C, we obtain

$$\frac{1}{2}\rho {u_{T_i}}^2 \sim \frac{\sigma}{r_{b_i}}, \tag{40}$$

where r_{b_i} is the initial radius at the rim tip. From (40), we obtain

$$Ca_i \sim \sqrt{\frac{2}{\tilde{r}_{b_i}}}\, Oh, \tag{41}$$

where $\tilde{r}_{b_i} = r_{b_i}/R$, the dimensionless initial radius of the rim tip. A comparison of (41) and (37) gives

$$\tilde{r}_{b_i} \simeq 3 \times 10^{-2}. \tag{42}$$

Using (37) and (42), we get the initial Reynolds number of retraction of the rim tip $Re_i = \rho u_{T_i} r_{b_i}/\mu$ as

$$Re_i \simeq \frac{0.24}{Oh}. \tag{43}$$

Since the hole expansion Reynolds numbers Re_o decrease with time starting from these Re_i, when $Re_i \sim 1$, viscous effects will be important from the beginning of hole expansion. According to (43), $Re_i \simeq 1$ when $Oh \simeq 0.24$; Fig. 10 shows this viscous limit of the present scaling laws by the vertical dashed–dotted line. For $Oh > 0.24$, one would expect the initial retraction velocity to scale as $u_{\mu\sigma}$, implying that Ca_i = constant, whose value is shown in Fig. 10 to be equal to 2, and the temporal evolution of hole expansion velocity in this viscous regime is then expected to obey the scaling laws proposed by Savva and Bush[16] and Munro *et al.*[22] No sharp swell is seen in this viscous regime, as could be seen comparing points A and B in Fig. 11.

For $Oh < 0.24$, viscous effects will not be important from the beginning of hole expansion, but will become important at some time when $Re_o = \rho u_o R/\mu \sim 1$. Replacing u_o in $Re_o \sim 1$ with (35) and rewriting the resulting expression in terms of Oh, the corresponding dimensionless time beyond which viscous effects will become important is

$$t_v^* = t^*|_{Re_o \sim 1} \simeq \left(\frac{c_5}{Oh}\right)^{7/3}. \tag{44}$$

For $0.003 \leq Oh \leq 0.055$, the range of Oh of the present study, $1.72 \times 10^3 < t_v^* < 1.53 \times 10^6$. These times are a few orders larger than our range of t^* (see Figs. 8 and 9) so that viscous effects could be neglected in our analysis. The corresponding dimensionless excess radii at which the present scaling will have to be modified to include viscous effects could be calculated from (44) by using (29) as

$$\tilde{r}_{ev} = \tilde{r}_e|_{Re_o \sim 1} \simeq \frac{c_3 c_5^{4/3}}{Oh^{4/3}}. \tag{45}$$

For the present range of Oh, $162 < \tilde{r}_{ev} < 7853$, is much larger than the range of $\tilde{r}_e$, as shown in Fig. 8. The present scaling is expected to be valid up to a dimensionless excess radius given by (45).

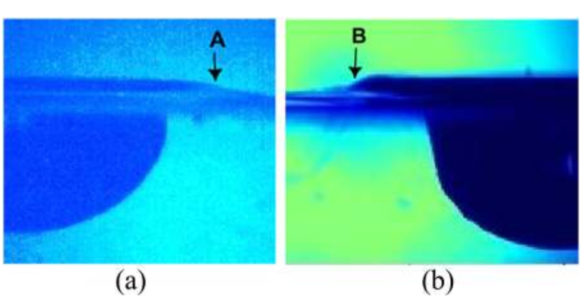

FIG. 11. Comparison of the swell in a high viscosity fluid with that in water at approximately 1.4 ms after the thin film rupture. (a) A smooth swell for R = 2.4 mm (Oh = 0.27, $R/R_{\mu\sigma}$ = 13.7) in GW86.8. Image width is 5.1 mm. (b) A sharp swell for R = 2.32 mm (Oh = 0.0025, $R/R_{\mu\sigma} = 16 \times 10^4$) in water. Image width is 4.63 mm.

V. DISCUSSION AND CONCLUSIONS

The primary contribution of the present paper is the finding of a novel $t^{4/7}$ dependence of the outer radius r_o on time t during the expansion of a hole at a liquid surface from bubble collapse at that surface. The physical explanation for this scaling is embodied in the scaling analysis presented in this paper. Such a scaling, different from the usually observed $t^{1/2}$ scaling of the neck radius in drop/bubble coalescence[18] as well as in the linear growth of hole in thin films of constant thickness[10,11] and the hole expansion in drop impact into a pool,[35] is seen in millimeter-sized bubbles at the surface of low viscosity fluids. In such bubbles, the retraction of the static rim of the bubble, after the initial viscous regime, results in the hole expansion at the free surface in a regime of low Ohnesorge numbers (Oh), high Reynolds numbers (Re_o), and low Capillary numbers (Ca_o); surface tension and inertia dominate the dynamics in this intermediate regime of hole expansion.

In such a regime, the surface tension force at the tip of the rim, which retracts the rim, is a function of the rim tip radius r_b, which itself varies with time as $r_b \sim r_T^{3/2}/\sqrt{R}$ due to the accumulation of mass at the rim tip, where r_T is the radial distance of travel along the interface from the initial static rim position. We show that when this surface tension force balances the unsteady inertia at the tip, the $t^{4/7}$ scaling occurs to yield $r_T \sim \left((u_c t)^4 R^3\right)^{1/7}$ (26), a function of two length scales $u_c t$ and R, where u_c is the capillary velocity. Since $r_T \simeq r_o - R_r = r_e$, the horizontal radius of the dynamic rim in excess of the initial static rim radius R_r, the variation of r_o with time then also shows a strong gravity dependence. The gravity dependence of r_o is because R_r is a strong function of Bond number (Bo), as given by Puthenveettil *et al.*[36] (1). The dimensionless scaling of the excess dynamic rim radius is then $r_e/R \sim t^{*4/7}$ (29), where $t^* = t/t_c$, with t_c being the inertial-capillary time scale. Hence, the gravity effects in the radius evolution come through the initial condition as an addition of the starting, constant, radius of the static rim R_r. This strong dependency on initial conditions for the evolution of r_o is a major feature of the present problem, in contrast to the universality and initial condition independence proposed for other bridge/neck expansion or neck pinching problems. Since R_r is independent of time, the scaling of velocity, however, becomes independent of gravity effects to give $u_o \sim \left(u_c^4 (R/t)^3\right)^{1/7}$ (35), a function of two velocity scales u_c and R/t; the corresponding Weber number of hole expansion scales as $We_o \sim t^{*^{-6/7}}$ (34).

These scalings of the hole radius and velocity of hole expansion occur during an intermediate period of the whole process of hole expansion from bubble collapse. The initial hole expansion occurs in the thin film cap and occurs with the well-known Taylor–Culick velocity $U_{TC} = \sqrt{2\sigma/\rho h}$,[7] with h being the film thickness. Since $h \approx 50$ nm for 1 mm water bubbles, $U_{TC} \approx 38$ m s^{-1}, a high velocity that is about an order of magnitude larger than the initial velocities of hole expansion in the present case; the film then disintegrates before it reaches the static rim. This disintegration could be the reason for our finding, implied in the above scaling law, that the static rim retracts without showing any effect of the high U_{TC} on the thin film cap.

The present evolution of the hole radius from a free surface bubble at intermediate times, since it occurs at low Oh and large Re_o, could be described by an inviscid dynamics. However, at the very beginning of the retraction of the static rim, due to the very thin rim thickness, a viscous regime could be present in the hole expansion dynamics, as suggested in the case of drop coalescence by Eggers, Lister, and Stone;[24] the retraction would then occur with a constant velocity of $u_{\mu\sigma} = \sigma/\mu$, neglecting logarithmic corrections. This regime is, however, inaccessible to optical investigations since the regime occurs within a viscous length scale $R_{\mu\sigma} = \mu^2/\rho\sigma$ of nanometers. The regime considered in the present study is expected to occur at intermediate times after the Taylor–Culick regime in the thin film cap and the very short viscous regime in the rim are over. The initial velocities of the present regime u_{T_i} would then scale as the capillary velocity, with the corresponding Weber number, We_i, being a constant (38). Starting from these capillary velocities, the Weber numbers of hole expansion decay with a $t^{-6/7}$ dependence.

Since the velocity of hole expansion decays with time, one would expect the viscous effects to become important in the hole expansion at large times, at which point the dynamics is expected to deviate from the present scaling laws. This would occur when $Re_o \sim 1$, the corresponding time would be $t_v \sim t_{\mu\sigma}/Oh^{16/3}$, where $t_{\mu\sigma} = \mu^3/\rho\sigma^2$ is the viscous-capillary time scale. Since t_v is a few orders larger than the present measurement times, the present dynamics remain inviscid. However, with an increase in viscosity of the fluids, and correspondingly Oh, t_v would decrease sharply and, hence, in highly viscous fluids, viscous effects would be significant even at the intermediate times of the present scaling; the dynamics would then deviate from that in the present regime even at intermediate times. The dynamics would be viscous from the beginning of the hole expansion itself when the Reynolds number in terms of the initial velocity and the rim tip radius Re_i is of order one. We estimate that such a viscous regime would occur for $Oh > 0.24$ and the images from the hole expansion in an experiment at $Oh = 0.27$ show the absence of the swell that propagates. The scaling of hole expansion in these viscous regimes is, however, unclear, but expected to be similar to that in the viscous regimes investigated by Munro *et al.*[22] for bubble coalescence.

ACKNOWLEDGMENTS

The authors would like to acknowledge the partial financial support from DST, Government of India, under the FIST Grant (Grant No. SR/FST/ETII-017/2003) and the Core Research Grant (Grant No. SR/S3/MERC/028/2009), for this study. S.K. gratefully acknowledges the fellowship from DAE, Government of India.

APPENDIX A: REASON FOR $\tilde{r}_1$ TO FOLLOW (1)

If t_1 is the time for the retraction to occur from the static rim of radius R_r to r_1, the dimensionless radius of the first point of our measurement of the retracting rim is

$$\tilde{r}_1 = \tilde{R}_r + \tilde{r}_T|_{t=t_1} \sin\phi. \tag{A1}$$

Since $\sin\phi = 1 - (\tilde{R}_r/2)^2$ for small Bo (see Ref. 36) and $\tilde{r}_T = c_3(t/t_c)^{4/7}$ from (26), at time t_1, (A1) becomes

$$\tilde{r}_1 = \tilde{R}_r\left(1 - \frac{c_3}{4}(t_1/t_c)^{4/7}\tilde{R}_r\right) + c_3(t/t_c)^{4/7}. \tag{A2}$$

For the points shown in the inset of Fig. 5, $t_1/t_c \leq 4 \times 10^{-2}$. Hence, $t_1/t_c \ll 1$, implying that $\tilde{r}_1 \simeq \tilde{R}_r$ as per (A2); $\tilde{r}_1$ then also follows (1).

APPENDIX B: TIME SCALE OF THIN FILM FRAGMENTATION

Considering only the inertial destabilization of Rayleigh–Taylor type, the time for the growth of instability in the thin film cap, as given by Lhuissier and Villermaux,[7] is

$$\tau \sim \sqrt{Bo_c}\left(\frac{\sqrt{h^3/R_c}}{g}\right)^{1/2}, \tag{B1}$$

where R_c is the cap radius [see Fig. 2(b)] and $Bo_c = \rho g R_c^2/\sigma$. The distance from the top of the thin film cap to the rim is $S = \theta_c R_c$, where θ_c is the angle that the rim makes with the vertical [see Fig. 2(a)]; $\theta_c \simeq \sin\theta_c = R_r/R_c = \sqrt{Bo/3}$ from Puthenveettil *et al.*[36] Then, the time for travel of the hole from the top of the cap to the rim is

$$t_c = S/U_{TC} \sim Bo_c\sqrt{\frac{h}{g}}. \tag{B2}$$

The thin film cap would have fully fragmented, if

$$\tau/t_c \sim \frac{1}{\sqrt{Bo_c}}\left(\frac{h}{R_c}\right)^{1/4} \ll 1. \tag{B3}$$

In our experiments, 1.5 nm $< h <$ 0.26 μm, 0.35 mm $< R_c <$ 3.2 mm, and $0.02 < Bo_c < 1.4$, resulting in $0.08 < \tau/t_c < 0.35$; (B3) is hence always satisfied in the present study. In addition to the Rayleigh Taylor instability, the disintegration of the thin film is also aided by other mechanisms such as Kelvin Helmholtz instability and centrifugal instability due to travel over a curved path and fast escape of the gas inside the bubble. Hence, the estimate (B1) of the time taken for the thin film cap to disintegrate is an overestimate, implying that the thin film would definitely have disintegrated due to fragmentation by the time the hole grows to reach the static rim. In agreement with the above estimate and with the observations of Lhuissier and Villermaux[7] and Krishnan, Hopfinger, and Puthenveettil,[42] we also observed that the thin film was fully aerosolized by the time the hole growth reached the static rim.

APPENDIX C: UNCERTAINTY IN THE ORIGIN OF TIME

We fix the origin of time (t = 0) as the instant at which the film has vanished and the static rim is exposed. Even though the fast retraction of the rim is captured with a high frame rate (≤19 000 fps and ≤100 000 fps), the images could still miss, in some cases, the exact instant at which the static rim is exposed. In such cases, $t = 0$ is taken as that instant corresponding to the next available image after the film has vanished, which would, however, actually be at a time interval δt after the actual instant at which the static rim is exposed. Such an offset in the origin of time could result in a deviation of the measured scaling relation of r_e vs t with the actual scaling relation. Let R_0 be the measured radius corresponding to the measured $t = 0$, while the radius at the actual $t = 0$ is R_r. We calculate δt as the time taken for the radius to expand from R_r to R_0, using the rim expansion velocity (38) and the value of R_r from (1). The deviation in the scaling law of r_e due to the uncertainty in the origin of time could be found by plotting r_e vs $t_n = t - \delta t$ along with the plot of r_e vs t. Figure 12 shows such a plot, where the black circles show r_e vs t, while the blue circles show r_e vs t_n. A slight deviation in the scaling of r_e vs t_n is seen only in the initial part of the data, with the latter part aligning with r_e vs t, which follows the 4/7 power law scaling. Even in the initial part of the data, the deviation due to the uncertainty in the origin of time takes the data farther away from the $t^{1/2}$ scaling, with the r_e vs t_n showing a much closer match with the $t^{4/7}$ scaling than the $t^{1/2}$ scaling.

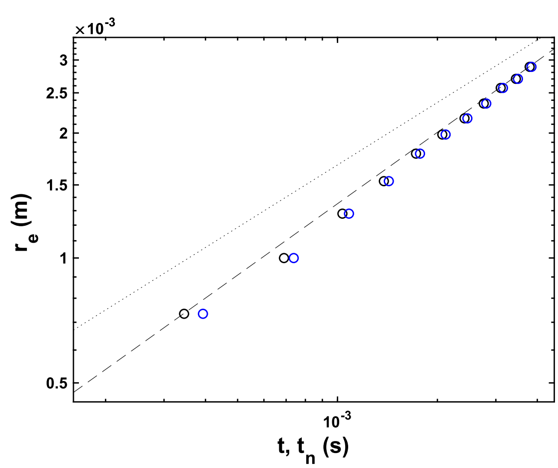

FIG. 12. Effect of uncertainty in the origin of time on the variation of the excess radius (r_e) for R = 2.32 mm in water. Black circles, r_e vs t, same as the data shown in Fig. 7; blue circles, r_e vs t_n, where $t_n = t - \delta t$; – –, 0.07 $t^{4/7}$; and . . ., 0.053 $t^{1/2}$.

APPENDIX D: THE LIMITING NO-BULGE CASE

For the case of rim retraction without formation of a bulge at the retracting rim tip, we expect the retraction geometry to be as shown in Fig. 13. In such a situation, the RHS of (3) reduces to $\pi r_b^2 2\pi r_r/2$, while the angle $2\theta \to \pi$. The surface area of the retracting rim tip (6) then reduces to

$$s = 2\pi^2 r_b^2 \tag{D1}$$

so that the force (7) becomes

$$\Sigma \overline{F}_r = 2\pi^2 r_b \sigma. \tag{D2}$$

The fictitious force due to the deceleration of the CV (8) now becomes

$$m\bar{a}_r = \rho\pi^2 r_b^2 r_r \frac{d\bar{u}_T}{dt}, \tag{D3}$$

while the efflux of momentum (15) reduces to

$$\int_S \bar{v}_r \rho \bar{v}_r \cdot d\bar{S} = \rho u_T^2 2\pi^2 r_b^2. \tag{D4}$$

Substituting (5), (D2), (D3), (D4), (11), and (F6) into (4) and using $R_r/r_T \ll 1$, we obtain

$$P_1 \simeq \frac{2}{r_T} \quad \text{and} \quad Q_1 \simeq \frac{2\sigma R}{\rho r_T^3}, \tag{D5}$$

instead of (23) and (24). Solving (16) using (D5), we obtain

$$\frac{u_T}{u_c} = c_7 \, \frac{R}{r_T}, \tag{D6}$$

where $c_7 = \sqrt{2}$. As earlier, using (9) and (D6), we obtain

$$\tilde{r}_T = c_8 \, t^{*^{1/2}}, \tag{D7}$$

the conventional inertial bubble coalescence scaling first proposed by Keller,[25] where $c_8 = 2^{3/4}$. Such a scenario is likely to occur at the beginning of hole expansion, especially for a low Oh case, since a bulge would soon form at the retracting tip to result in the 4/7 scaling given by (26).

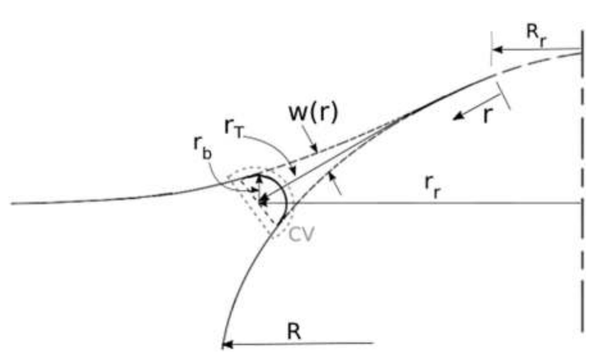

FIG. 13. Schematic showing the retracted rim without a growing bulge at its tip.

APPENDIX E: A MODIFIED EULER EQUATION APPROACH

In this section, we show that the scaling (26) can be obtained in a simpler way by applying a modified Eulers equation at a point inside the retracting bulge at the rim tip. We then generalize this approach to obtain all the well-known classical scaling laws in hole expansion.

1. Obtaining (26)

The temporal acceleration of the rim expansion $\partial u_o/\partial t \sim u_o/(2r_b/u_o) = u_o^2/(2r_b)$ because the swell of diameter $2r_b$ travels with a velocity u_o. The spatial acceleration of hole expansion is $u_o\partial u_o/\partial r \sim u_o^2/r_o$. The ratio of temporal to spatial acceleration of hole expansion then scales as $r_o/r_b \gg 1$ for the long term evolution of r_o; the spatial acceleration terms could then be neglected. For low Oh of the present study, the spatial gradients of velocity inside the retracting bulge are negligible, as could be seen from Savva and Bush;[16] this again justifies neglecting the convective acceleration term. As discussed in Sec. IV, viscous effects in the hole expansion process could be neglected given that $Re_o \sim 10^3$ and that $Oh \sim 10^{-3}$ (see Table II). A similar approach has been used earlier to study the rim retraction problems.[43] Under such conditions, at any point inside the bulge at the expanding hole edge, the reduced equation that decides the hole expansion is then

$$\frac{\partial u_T}{\partial t} = \frac{1}{\rho}\frac{\partial p}{\partial r_T}, \tag{E1}$$

where u_T is given by (9).

In (E1), the pressure inside the bulge at the rim tip or the swell traveling along the free surface is

$$p = \frac{\sigma}{r_b}. \tag{E2}$$

Using (E2) and (12) in (E1), simplifying, and then integrating, along with the condition that $u_T \to 0$ as $r_T \to \infty$, result in the dimensionless rim tip retraction velocity,

$$\frac{u_T}{u_c} = c_9\left(\frac{R}{r_T}\right)^{3/4}, \tag{E3}$$

where $c_9 = \sqrt{2/c_1} = 2.67$. Substituting (9) in (E3), rearranging, and integrating, along with using $r_T \to 0$ as $t \to 0$, we obtain

$$\tilde{r}_T = c_{10}\, t^{*\,4/7}, \tag{E4}$$

where $c_{10} = (7c_9/4)^{4/7} = 2.4$.

The evolution equation for r_T, of which (E4) is a solution, could be obtained by substituting (9), (E2), and (12) in (E1) as

$$\frac{d^2 r_T}{dt^2} + \frac{3}{2c_1}\frac{\sigma\sqrt{R}}{\rho}\frac{1}{r_T^{5/2}} = 0. \tag{E5}$$

Equation (E5) shows that the non-linear evolution of r_T seen in (E4) occurs due to the second term in (E5), which represents the evolution of pressure at the retracting rim tip. This non-linear evolution of pressure occurs owing to the evolution of the curvature at the tip of the retracting rim (12), which again depends on how the mass accumulates at the tip of the retracting rim. The accumulated mass and the resulting radius of the bulge at the tip of the retracting rim r_b, in turn, depend on the static bubble geometry through a mass balance, as shown in Appendix F.

2. Generalization

We now extend the above analysis to obtain a general scaling relation for the dependence of the radius of the hole on time for arbitrary power law variations of the film thickness and the bulge radius; the well-known hole expansion scaling laws such as Taylor–Culick scaling law,[10,11] Keller's scaling,[25] and the inertial coalescence scaling[22,24,25,28] can be obtained from this general scaling law for specific assumptions about the film thickness h and the radius at the tip of the retracting film r_b.

Let the thickness of the film be

$$h = a_1 r_T^{\alpha}, \tag{E6}$$

where a_1 is a prefactor with dimension $L^{1-\alpha}$ and α is a power law exponent with real values. To obtain a generalized scaling for the hole expansion, we assume a general geometry of the bulge at the tip of the retracting film as follows. Let the bulge radius at the tip of the retracting film scale as

$$r_b = a_2 r_T^{\beta} h^{1-\beta}, \tag{E7}$$

where a_2 is a dimensionless prefactor and β is a power law exponent with real values. The power law scaling of r_b on r_T and h has to be of the form (E7) for dimensional consistency. Expressions (E7) and (E6) imply that

$$r_b = a_2 a_1^{1-\beta} r_T^{\xi}, \tag{E8}$$

where $\xi = \beta + \alpha(1-\beta)$. By replacing the pressure at the tip of the retracting film in [(E1)] with $p = \sigma/r_b$, with r_b given by (E8) and differentiating RHS with respect to r_T, we obtain

$$\frac{\partial u_T}{\partial t} = \frac{d^2 r_T}{dt^2} = -\frac{\xi\sigma}{\rho a_2 a_1^{1-\beta} r_T^{\xi+1}}. \tag{E9}$$

The differential equation (E9) is the evolution equation of r_T for the general power law variations of h and r_b given by (E6) and (E7), respectively.

Rewriting the LHS of (E9) as $(du_T/dr_T)u_T$ and integrating, along with the condition that $\lim_{r_T\to\infty} u_T = 0$, gives

$$u_T = \frac{\Gamma}{r_T^{\zeta}}, \tag{E10}$$

where

$$\Gamma = \sqrt{\frac{2\sigma}{\rho a_2 a_1^{1-\beta}}} \tag{E11}$$

and

$$\zeta = \frac{\xi}{2}. \tag{E12}$$

Integrating (E10) with respect to t along with the condition that $\lim_{t\to 0} r_T = 0$, we obtain

$$r_T = ((\zeta+1)\Gamma t)^{1/(\zeta+1)}, \tag{E13}$$

where Γ is given by (E11) and ζ by (E12). Equations (E13) and (E10) are the general expressions for the radius of the hole and its velocity of expansion for a film/rim, whose thickness varies as (E6) and whose radius of the bulge at the tip of the retracting film/rim scales as (E7). It needs to be noted that the general scaling laws (E10) and (E13) are obtained from the momentum balance alone; the same is the case for the scalings obtained by Culick[11] and Keller[25] where, in addition, consideration of bulge formation is also not included, as shown in Appendix H. The expressions (E10) and (E13) just tell us that if the film thickness varies as (E6) and the bulge radius as (E7), then the hole radius will scale as (E13). The value of r_b that occurs in a specific case of hole expansion has to be obtained by augmenting the momentum balance implied in (E1) with a mass balance condition capturing the balance of accumulation at the tip and a flow along the film, as we obtain the present scaling in Appendix E 3 d.

3. Retrieving classical scaling laws from (E13)

We can now obtain the various well-known hole expansion scalings from the general scaling laws (E10) and (E13), as shown below.

a. Taylor–Culick scaling[10,11]

When $\alpha = 0$, $\beta = 0$, and $a_2 = 1$, the bulge radius (E7) becomes $r_b = h$ and (E10) becomes the Taylor–Culick velocity for the retraction of a thin film of uniform thickness $h = a_1$,

$$u_T = \sqrt{\frac{2\sigma}{\rho h}}. \tag{E14}$$

b. Keller's scaling[25]

By using $\beta = 0$ and $a_2 = (\alpha + 4)/(2(\alpha + 2))$ in (E13), we obtain

$$r_T(t) = t^{2/(2+\alpha)}\left(\frac{\sigma(\alpha+2)^3}{\rho a_1(\alpha+4)}\right)^{1/(2+\alpha)}, \tag{E15}$$

Keller's scaling,[25] a general scaling law for the hole radius of a retracting film, whose thickness scales as (E6).

c. Inertial-capillary coalescence scaling

For the film thickness to vary as (E6), $\alpha = 2$ and $a_1 = 1/R$. Now, if $\beta = 0$ and $a_2 = 1/2$ in (E7), we obtain $r_b = h/2$, implying that there is no bulge formation at the retracting film tip. Using these values of α, β, a_1, and a_2 in (E13), we obtain the conventional inertial coalescence scaling for hole expansion in the case of two merging bubbles,

$$r_T(t) = 2\left(\frac{\sigma R}{\rho}\right)^{1/4}\sqrt{t}. \tag{E16}$$

d. The present scaling

The mass balance of the retracting rim, as described in Appendix F, results that the bulge radius should be given by (12) with $c_1 = 1/2\sqrt{\pi}$. Comparing (12) and (E7), as well as (F6) and (E6), implies that $\alpha = 2$, $\beta = 1/2$, $a_1 = 1/R$, and $a_2 = c_1$ for the present case. Substituting these values in (E13) results in

$$r_T = \left(\frac{49}{8c_1}\right)^{2/7}\left(\frac{\sigma\sqrt{R}}{\rho}\right)^{2/7} t^{4/7}, \tag{E17}$$

the same as (E4). To apply Keller's result (E15) in the present problem, for the present case of variation of the film/rim thickness given by (F6), a comparison of (F6) and (E6) implies that $\alpha = 2$ and $a_1 = 1/R$. However, substituting these values in (E15) results in the conventional inertial coalescence scaling (E16), different from the $t^{4/7}$ scaling that we observe. Hence, for the expected variation of film/rim thickness given by (F6), Keller's scaling will be unable to recover the observed $r_T \sim t^{4/7}$ scaling in the present case since they neglect the change in the force of retraction owing to the change in the curvature of the retracting film tip due to the formation of a bulge at the tip of the retracting rim.

APPENDIX F: MASS BALANCE OF THE RETRACTING RIM

At any time t, the amount of liquid that was in the meniscus between the static rim position and the position of the bulge gets accumulated in the bulge of radius r_b, implying

$$\int_0^{r_T} 2\pi r_i w(r)dr = \pi r_b^2 2\pi r_r. \tag{F1}$$

From the geometry shown in Figs. 2(b) and 2(a),

$$\sin\phi = \frac{r_r - R_r}{r_T} \simeq \frac{R_c - h_{cap} - R}{R}, \tag{F2}$$

implying that $\sin\phi \simeq \tilde{R}_c - \tilde{h}_{cap} - 1$. For $Bo < 1$, $\tilde{h}_{cap} = Bo/3$, and for small Bo, $\tilde{R}_c = 2$[36,44] so that

$$\sin\phi \simeq 1 - Bo/3. \tag{F3}$$

Using (F3) in the relation $r_i = r\sin\phi + R_r$, we obtain

$$r_i \simeq r(1 - \frac{1}{3}Bo) + R_r. \tag{F4}$$

As shown in Fig. 2(b),

$$w = 2R(1 - \cos\theta_r). \tag{F5}$$

Since for small θ_r, $\cos\theta_r = 1 - \theta_r{}^2/2$ and $\sin\theta_r = r_T/R \simeq \theta_r$, (F5) implies that

$$w(r) = r^2/R. \tag{F6}$$

Substituting w from (F6), r_i from (F4), and r_b from (12) in (F1) and integrating result in the bulge radius

$$r_b \simeq \frac{r_T{}^{3/2}}{\sqrt{3\pi R}}\chi, \tag{F7}$$

where

$$\chi = \sqrt{\frac{3}{4}}\sqrt{\frac{4 + (3 - Bo)r_T/R_r}{3 + (3 - Bo)r_T/R_r}}. \tag{F8}$$

Since $r_T/R_r \gg 1$, the term in the second square root in (F8) is of order one, implying that

$$\chi \simeq \frac{\sqrt{3}}{2}. \tag{F9}$$

Using (F9) in (F7) implies that

$$r_b \simeq c_1 \frac{{r_T}^{3/2}}{\sqrt{R}}, \tag{F10}$$

where

$$c_1 = \frac{1}{2\sqrt{\pi}}. \tag{F11}$$

APPENDIX G: EXPANSION OF SWELL

In our analysis, the radius of the outer edge of the swell r_o was used as an estimate of the hole radius, since the inner radius of the swell, which is the actual hole radius, is not visible in the side view images. If the swell changes its size over the time of measurement of r_o, then using r_o to estimate the hole radius would introduce an error. We now estimate the condition for neglecting the expansion of the swell, which satisfies our range of analysis. The rate of change of the swell radius is

$$u_{r_b} = \frac{dr_b}{dt} = \frac{dr_b}{dr_T}\frac{dr_T}{dt}. \tag{G1}$$

Using (9) and (12) in (G1) yields

$$\frac{u_{r_b}}{u_T} = \frac{3}{2}c_1\left(\frac{r_T}{R}\right)^{1/2}, \tag{G2}$$

where $c_1 = 1/2\sqrt{\pi}$. Since $r_T \simeq r_o - R_r = r_e$ in (G2), the condition for neglecting the swell expansion in comparison to the hole expansion, $u_{rb}/u_T < 1$, results in

$$\tilde{r}_e = \frac{r_e}{R} < 5.6. \tag{G3}$$

Our range of analysis satisfies (G3), as could be seen in Fig. 8, so as to neglect the swell expansion.

APPENDIX H: TAYLOR–CULICK AND KELLER'S SCALING

The Taylor–Culick velocity[11] U_{TC} of hole expansion in a thin film of uniform thickness h was obtained as follows. At any time, the retracting mass m in a sector of angle κ of the film was estimated as the mass of the undisturbed film that had occupied at previous times in the sector over a radius equal to the hole radius r_h, i.e.,

$$m = \rho h r_h^2 \kappa/2. \tag{H1}$$

The rate of change of momentum of this retracting fluid, retracting with a constant velocity U_{TC} at any time,

$$\frac{d(mU_{TC})}{dt} = \frac{d(mU_{TC})}{dr_h}U_{TC} = m\frac{d(U_{TC}^2/2)}{dr_h} + U_{TC}^2\frac{dm}{dr_h}, \tag{H2}$$

where $U_{TC} = dr_h/dt$ and the first term is retained even though U_{TC} is assumed to be constant with t and r_h. Using product rule, (H2) can be written as

$$\frac{d(mU_{TC})}{dt} = \frac{d(mU_{TC}^2/2)}{dr_h} + \frac{U_{TC}^2}{2}\frac{dm}{dr_h}. \tag{H3}$$

Using (H1) in (H3), we obtain

$$\frac{d(mU_{TC})}{dt} = \rho r_h h \kappa U_{TC}^2. \tag{H4}$$

When (H4) is equated to the force due to surface tension

$$F = 2\sigma r_h \kappa, \tag{H5}$$

we obtain the well-known expression $U_{TC} = \sqrt{2\sigma/\rho h}$.

It needs to be noted that even though most papers state that Culick's derivation assumes that the mass m accumulates at the retracting tip, in the above derivation, there is no assumption about what happens at time t to the mass that had occupied in the sector of volume $r_h^2\kappa h/2$ of the film at previous times. In other words, mass balance at time t is not used in this derivation. Furthermore, F given by (H5) is obtained when a horizontal force/length of σ acts on the edge of a retracting film of length $r_h\kappa$ on the top and bottom of the retracting film. Such a force acting on the retracting mass is possible only when the retracting fluid does not form a bulge at the retracting tip. In other words, for the retracting force to be that given by (H5), the inherent assumption in the derivation is that there is no bulge formation due to the accumulation of fluid at the retracting tip. Such an inherent assumption would mean that there has to be a flow along the film to satisfy the mass balance.

Similar is the case with Keller's derivation of the $r_h \sim t^{1/2}$ scaling of the hole radius in coalescing bubbles. Keller uses the momentum balance alone in the form

$$\frac{d}{dt}\left(\rho\int_0^{r_h(t)} 2\pi r w(r) dr \frac{dr_h}{dt}\right) = 4\sigma\pi r_h(t), \tag{H6}$$

after neglecting $1/\sqrt{1 + \left(\frac{1}{2}\partial w/\partial r|_{r=r_h}\right)^2}$, the curvature at the retracting rim tip on the RHS of (H6). This implies that such an analysis is valid only when

$$\left.\frac{\partial w}{\partial r}\right|_{r=r_h} \ll 2. \tag{H7}$$

Using $w(r) = r^2/R$, (H7) implies that Keller's scaling, even in the absence of any bulge formation, is valid only until $r_h \ll R$.

Now, in the presence of bulge formation at the retracting rim tip due to the accumulation of retracting fluid, assuming the bulge to be toroidal, $\partial w/\partial r|_{r=r_h} = \infty$, clearly violating the condition (H7) for the validity of Keller's analysis. Hence, since the RHS of (H6) is the surface tension force in the absence of bulge formation, Keller's scaling is expected when the rim retracts with no bulge formation. In such a case, except in the beginning of retraction, which we discuss in Appendix D to show that $t^{1/2}$ is still possible, there has to be a flow along the film to conserve the mass. Keller's analysis does not specify the state at time t of the mass that occupied the undisturbed film from 0 to r_h in previous times; the scaling has no mass conservation in it. Due to these reasons, the scaling proposed by Keller will deviate from the scaling of hole expansion in the presence of bulge formation, which we discuss in Sec. IV.

APPENDIX I: MEASUREMENT OF INITIAL VELOCITY

The initial velocity u_{Ti} is measured as follows. The static rim position is first observed from the images before the bubble bursts.

The hole expansion in the thin film cap is then tracked. We observe no bulge formation as long as $r_o < R_r$, while in the first image for which $r_o > R_r$, we observe a bulge at the rim tip. The distance along the travel path of the retraction between the last image for which $r_o < R_r$ in which no bulge forms and the first image for which $r_o > R_r$ in which a bulge forms is then measured. u_{Ti} is calculated as this distance divided by the time between the frames.

This measurement of u_{Ti} is, hence, an average velocity measured over a very short distance before the rim, where no bulge forms in the retracting film and a very short distance after the rim, where a bulge is seen forming in the retracting rim. This measurement of u_{Ti} would give a reasonably accurate estimate of the initial velocity of the rim if the time over which u_T changes at the initial time $t = t_i$,

$$\delta t_i = \frac{u_{Ti}}{du_T/dt|_{t=t_i}} \ll \Delta t, \tag{I1}$$

the time between frames. Estimating $du_T/dt|_{t=t_i}$ as $(U_{TC} - u_1)/\Delta t$, where u_1 is the first measured u_o (corresponding to r_1 in Fig. 5) is satisfied when

$$u_{Ti}/(U_{TC} - u_1) \ll 1. \tag{I2}$$

We find that the values of $u_{Ti}/(U_{TC} - u_1)$ are of the order of 10^{-2} in our measurements, implying that the error in approximating the average measured value of u_{Ti} as the initial velocity of retraction of rim is small.

REFERENCES

[1] A. K. Gupta, B. K. Saxena, S. N. Tiwari, and S. L. Malhotra, "Pore formation in cast metals and alloys," J. Mater. Sci. **27**, 853–862 (1992).
[2] R. S. Cherry and C. T. Hulle, "Cell death in the thin films of bursting bubbles," Biotechnol. Prog. **8**, 11–18 (1992).
[3] T. V. Vinay, T. N. Banuprasad, S. D. George, S. Varghese, and S. N. Varanakkottu, "Additive-free tunable transport and assembly of floating objects at water-air interface using bubble-mediated capillary forces," Adv. Mater. Interfaces **4**, 1601231 (2017).
[4] J. Feng, M. Roché, D. Vigolo, L. N. Arnaudov, S. D. Stoyanov, T. D. Gurkov, G. G. Tsutsumanova, and H. A. Stone, "Nanoemulsions obtained via bubble-bursting at a compound interface," Nat. Phys. **10**, 606–612 (2014).
[5] I. Leifer and R. K. Patro, "The bubble mechanism for methane transport from the shallow sea bed to the surface: A review and sensitivity study," Cont. Shelf Res. **22**, 2409–2428 (2002).
[6] M. R. James, S. J. Lane, L. Wilson, and S. B. Corder, "Degassing at low magma-viscosity volcanoes: Quantifying the transition between passive bubble-burst and strombolian eruption," J. Volcanol. Geotherm. Res. **180**, 81–88 (2009).
[7] H. Lhuissier and E. Villermaux, "Bursting bubble aerosols," J. Fluid Mech. **696**, 5–44 (2012).
[8] D. Vaynblat, J. R. Lister, and T. P. Witelski, "Rupture of thin viscous films by van der Waals forces: Evolution and self-similarity," Phys. Fluids **13**, 1130–1140 (2001).
[9] S. S. Thete, C. Anthony, P. Doshi, M. T. Harris, and O. A. Basaran, "Self-similarity and scaling transitions during rupture of thin free films of Newtonian fluids," Phys. Fluids **28**, 092101 (2016).
[10] G. I. Taylor, "The dynamics of thin sheets of fluid. III. Disintegration of fluid sheets," Proc. R. Soc. London, Ser. A **253**, 313–321 (1959).
[11] F. E. C. Culick, "Comments on a ruptured soap film," J. Appl. Phys. **31**, 1128–1129 (1960).
[12] W. R. McEntee and K. J. Mysels, "Bursting of soap films. I. An experimental study," J. Phys. Chem. **73**, 3018–3028 (1969).
[13] A. B. Pandit and J. F. Davidson, "Hydrodynamics of the rupture of thin liquid films," J. Fluid Mech. **212**, 11–24 (1990).
[14] M. P. Brenner and D. Gueyffier, "On the bursting of viscous films," Phys. Fluids **11**, 737–739 (1999).
[15] G. Debrégeas, P.-G. de Gennes, and F. Brochard-Wyart, "The life and death of "bare" viscous bubbles," Science **279**, 1704–1707 (1998).
[16] N. Savva and J. W. M. Bush, "Viscous sheet retraction," J. Fluid Mech. **626**, 211–240 (2009).
[17] J. San Lee, B. M. Weon, S. J. Park, J. H. Je, K. Fezzaa, and W.-K. Lee, "Size limits the formation of liquid jets during bubble bursting," Nat. Commun. **2**, 367 (2011).
[18] J. D. Paulsen, R. Carmigniani, A. Kannan, J. C. Burton, and S. R. Nagel, "Coalescence of bubbles and drops in an outer fluid," Nat. Commun. **5**, 3182 (2014).
[19] J. D. Paulsen, J. C. Burton, S. R. Nagel, S. Appathurai, M. T. Harris, and O. A. Basaran, "The inexorable resistance of inertia determines the initial regime of drop coalescence," Proc. Natl. Acad. Sci. U. S. A. **109**, 6857–6861 (2012).
[20] J. D. Paulsen, J. C. Burton, and S. R. Nagel, "Viscous to inertial crossover in liquid drop coalescence," Phys. Rev. Lett. **106**, 114501 (2011).
[21] C. R. Anthony, P. M. Kamat, S. S. Thete, J. P. Munro, J. R. Lister, M. T. Harris, and O. A. Basaran, "Scaling laws and dynamics of bubble coalescence," Phys. Rev. Fluids **2**, 083601 (2017).
[22] J. P. Munro, C. R. Anthony, O. A. Basaran, and J. R. Lister, "Thin-sheet flow between coalescing bubbles," J. Fluid Mech. **773**, R3 (2015).
[23] D. G. Aarts, H. N. W. Lekkerkerker, H. Guo, G. H. Wegdam, and D. Bonn, "Hydrodynamics of droplet coalescence," Phys. Rev. Lett. **95**, 164503 (2005).
[24] J. Eggers, J. R. Lister, and H. A. Stone, "Coalescence of liquid drops," J. Fluid Mech. **401**, 293–310 (1999).
[25] J. B. Keller, "Breaking of liquid films and threads," Phys. Fluids **26**, 3451–3453 (1983).
[26] A. M. Soto, T. Maddalena, A. Fraters, D. van der Meer, and D. Lohse, "Coalescence of diffusively growing gas bubbles," J. Fluid Mech. **846**, 143–165 (2018).
[27] S. T. Thoroddsen, K. Takehara, and T. G. Etoh, "The coalescence speed of a pendent and a sessile drop," J. Fluid Mech. **527**, 85–114 (2005).
[28] L. Duchemin, J. Eggers, and C. Josserand, "Inviscid coalescence of drops," J. Fluid Mech. **487**, 167–178 (2003).
[29] H. N. Oguz and A. Prosperetti, "Dynamics of bubble growth and detachment from a needle," J. Fluid Mech. **257**, 111–145 (1993).
[30] P. Doshi, I. Cohen, W. W. Zhang, M. Siegel, P. Howell, O. A. Basaran, and S. R. Nagel, "Persistence of memory in drop breakup: The breakdown of universality," Science **302**, 1185–1188 (2003).
[31] L. Cheng-Yuan and J. C. Slattery, "Thinning of a liquid film as a small drop or bubble approaches a fluid–fluid interface," AIChE J. **28**, 786–792 (1982).
[32] P. Howell, "The draining of a two-dimensional bubble," J. Eng. Math. **35**, 251–272 (1999).
[33] C. T. Nguyen, H. M. Gonnermann, Y. Chen, C. Huber, A. A. Maiorano, A. Gouldstone, and J. Dufek, "Film drainage and the lifetime of bubbles," Geochem., Geophys., Geosyst. **14**, 3616–3631, https://doi.org/10.1002/ggge.20198 (2013).
[34] H. Kočárková, F. Rouyer, and F. Pigeonneau, "Film drainage of viscous liquid on top of bare bubble: Influence of the bond number," Phys. Fluids **25**, 022105 (2013).
[35] L. J. Leng, "Splash formation by spherical drops," J. Fluid Mech. **427**, 73–105 (2001).
[36] B. A. Puthenveettil, A. Saha, S. Krishnan, and E. J. Hopfinger, "Shape parameters of a floating bubble," Phys. Fluids **30**, 112105 (2018).
[37] M. L. Boas, *Mathematical Methods in the Physical Sciences* (John Wiley & Sons, 2006).
[38] V. Garg, P. M. Kamat, C. R. Anthony, S. S. Thete, and O. A. Basaran, "Self-similar rupture of thin films of power-law fluids on a substrate," J. Fluid Mech. **826**, 455–483 (2017).
[39] M. S. Longuet-Higgins and H. Oguz, "Critical microjets in collapsing cavities," J. Fluid Mech. **290**, 183–201 (1995).

[40] J. Lu and C. M. Corvalan, "Dynamical transitions during the collapse of inertial holes," Sci. Rep. **9**, 14649 (2019).
[41] J. R. Castrejón-Pita, A. A. Castrejón-Pita, S. S. Thete, K. Sambath, I. M. Hutchings, J. Hinch, J. R. Lister, and O. A. Basaran, "Plethora of transitions during breakup of liquid filaments," Proc. Natl. Acad. Sci. U. S. A. **112**, 4582–4587 (2015).
[42] S. Krishnan, E. J. Hopfinger, and B. A. Puthenveettil, "On the scaling of jetting from bubble collapse at a liquid surface," J. Fluid Mech. **822**, 791–812 (2017).
[43] S. Čopar and A. Kodre, "One-dimensional simulation of thin liquid-film-edge retraction," Phys. Rev. E **82**, 056307 (2010).
[44] H. M. Princen, "Shape of a fluid drop at a liquid-liquid interface," J. Colloid Sci. **18**, 178–195 (1963).